High-fidelity CFD Simulations of Two Wind Turbines in Arrays using Nonlinear Frequency Domain Solution Method

Shine Win Naung, Mahdi Erfanian Nakhchi, Mohammad Rahmati*
Department of Mechanical and Construction Engineering, Northumbria University, Newcastle upon Tyne NE1 8ST, United Kingdom

*Corresponding author
Email: mohammad.rahmati@northumbria.ac.uk

ABSTRACT

Aerodynamics of a wind turbine within windfarms is strongly influenced by the wake of neighbouring turbines. In particular, the performance of a wind turbine can be dramatically reduced depending on its location in the wake region of an upstream turbine. A detailed investigation of the effect of the upstream turbine on the downstream turbine with respect to their distances is essential for the design and optimisation of wind farm layouts. Conventional time domain solution methods, such as Unsteady Reynolds Averaged Navier Stokes (URANS) based Computational Fluid Dynamics (CFD) model of wind turbines in arrays, can provide a detailed analysis of this interaction effect. These methods are, however, impractical due to the high computational cost required for modelling turbines in array configurations. In this paper, a novel modelling and computational method is proposed to simulate two wind turbines in arrays by considering them as a multi-stage turbine. A nonlinear frequency domain solution method is then employed to model flow nonlinearities due to their interactions. The distances between the turbines are varied, and the effects of the upstream wind turbine on the downstream one are thoroughly investigated. Extensive validations of the nonlinear frequency domain solution method against the conventional time domain solution method reveal that the proposed frequency domain solution method provides accurate results while reducing the computational cost by one to two orders of magnitude.

Keywords: wind turbines in arrays, high-fidelity CFD, aerodynamics, frequency domain method, rotor-stator interaction, unsteady Navier-Stokes

1. INTRODUCTION

Wind energy is one of the most used green sources of electricity and has become popular as the wind is reliable and freely available [1]. Approximately 10 GW of electricity is produced from offshore wind, and combined offshore and onshore wind farms can provide power for more than 18 million homes every year in the UK. It is expected that over 10% of UK electricity will be generated from offshore wind in the next few years. To meet the increasing energy demand, the sizes of wind turbines are being increased to capture the wind more effectively and efficiently [2]. Although innovative technologies and advances in wind turbines play a vital role in the success of the wind energy industry, the design and optimisation of wind farms are challenging for the industry in order to maximize the energy captured as well as the power generation [3,4]. A wind farm consists of a number of large-capacity wind turbines and therefore, the flow around a turbine is expected to be influenced by the wakes from neighbouring turbines [5]. Among several factors to design and optimise a wind farm layout, the determination of separation distance between adjacent turbines is very crucial to minimize the influence of the wake deficits and turbulence from the upstream wind turbine and to maximize the power output of the downstream turbine [6]. Therefore, the wake calculation and prediction are of utmost importance to identify the effects associated with neighbouring wind turbines for the optimisation of the wind farm layout.

Ideally, the prediction of aerodynamic performances of wind turbines should be carried out or validated through full-scale experiments to achieve accurate results. While full-scale wind turbine experiments are not practically feasible, various small-scale experiments were conducted and reported in the literature [7-12]. Although researchers have control of inflow conditions or boundary conditions in the wind tunnel experiments, these experiments still impose uncertainties while reproducing the environmental conditions in which wind turbines are operated [13]. Therefore, the flow unsteadiness associated with these physical key factors is ignored in the wind tunnel experiments. Furthermore, the scaling effect encountered with the small-scale experiments should also not be neglected.

With all the advances in computing and technology, several numerical modelling and solution methods are now available for analysing the aerodynamics of wind turbines. Modern wind turbines are designed based on wind turbine specialist codes based on the Blade Element Momentum (BEM) theory [14]. The BEM models are typically used for the prediction of aerodynamic loads in the initial stage of the design process of wind turbine rotors and blades. However, the accuracy of the prediction depends on the availability of the aerofoil data for the lift and drag coefficients. The advantage of BEM models is computationally fast and reasonable results can be obtained provided that adequate aerofoil data are available. However, flow details, which is important for the aerodynamics of wind turbines, cannot be obtained with BEM models. Therefore, wind tunnel experiments or high-fidelity numerical methods are still required and usually employed in the later stage of the design process of wind turbines in order to understand the flow behaviour. The vortex models employing prescribed-wake methods or free-wake methods are also applied to the analysis of aerodynamics and wake structures of wind turbines. Lee et al. [15] used an unsteady vortex-lattice method to study the aerodynamic performance and wake structures of a wind turbine. Riziotis et al. [16] and Jeong et al. [17] applied a free-wake model to study the aerodynamics and aeroelasticity of wind turbine blades under different conditions. Rodriguez et al. [18,19] employed a vortex model for the aerodynamic analysis of offshore wind turbines. The viscous effects, however, are neglected by most vortex models. The actuator type models in which the wind turbine rotor or blades are represented by a disk or a line model with variable load distributions, known as the actuator disk model or actuator line model, are also used in the wind turbine aerodynamic analysis.

Sorensen et al. [20] used the actuator disk model to analyse the turbulent wake and vortex states of a wind turbine rotor whereas Troldborg et al. [21] applied the actuator line model to the simulation of a wind turbine operating in the turbulent wake. These methods can be combined with Navier-Stokes equations replacing the rotor or the blade with an actuator disc or line with distributed loads. However, the loads on the rotor or the blade are calculated based on the BEM theory and the accuracy of the simulation depends on the calculation of the aerodynamic loads. In addition, the computational costs required by these methods are higher than BEM models [22].

Computational Fluid Dynamics (CFD) methods can resolve the flow structures and boundary layers without requiring the load prediction on the blade surfaces or aerofoil data beforehand. Recently, CFD methods are used in the wind energy industry to analyse as well as optimise aerodynamic performances of wind turbines [23-25]. Lin et al. [26] and Dose et al. [27] used a CFD model to calculate aerodynamic loads on a wind turbine blade or rotor whereas Yu et al. [28] and Dose et al. [29] employed a CFD method to perform an aerodynamic analysis of a complete wind turbine model including a tower and predicted flow structures. CFD methods have also been applied to simulations of multiple wind turbines. Allah et al. [30] and Ciri et al. [31] conducted aerodynamic simulations of two in-line wind turbines and analysed the wake behaviour. Choi et al. [32] performed CFD simulations of two wind turbines by varying the separation distance between turbines. Moreover, Korobenko et al. [33] proposed a multi-domain method to perform simulations of two back-to-back wind turbines. The main disadvantage of the CFD methods is their large computational resources requirement. Significant computational resources and long runtimes are typically required for the unsteady computations, especially when multiple wind turbines are involved.

In the field of turbomachinery analysis, numerical studies have been conducted to develop efficient numerical methods which can reduce the computational cost without compromising accuracy in predicting unsteady flows. Frequency domain methods such as the harmonic balance method of Hall et al. [34], the phase solution method of He [35], and Rahmati et al. [36,37] have been developed and widely used in the turbomachinery analysis due to their capabilities of modelling harmonic disturbances and flow nonlinearities at a reasonable computational cost. It is also important to ensure that frequency domain methods can predict the flow structures accurately when highly unsteady flows are involved. High-resolution direct numerical simulations of the transitional flow structures around an aerofoil provides interesting and detailed vortex structures [38,39]. The capability of a frequency domain method on capturing these highly unsteady flow structures in a modern low-pressure turbine was also investigated by Shine et al. [40] by means of direct numerical simulation and it is found that it has the capability of predicting complex and highly unsteady flows.

Recently, frequency domain methods have also been applied to the aerodynamic and aeroelasticity analysis of wind turbines [41,42]. Shine et al. [43] proposed a nonlinear frequency domain solution method to analyse the effect of inflow turbulence and wake on both aerodynamics and aeroelasticity of wind turbine rotors, and also investigated the effect of material properties on the aerodynamic damping of the blade based on a relatively high amplitude of vibration. It appears that the inflow wake influences the flow field around the wind turbine, and it has an impact on both aerodynamics and aeroelasticity of the wind turbine blade. They later extended their study to carry out an aeromechanical analysis of a complete wind turbine model including a tower using a nonlinear frequency domain solution method [44]. Rahmati et al. [45] developed a nonlinear frequency domain solution method for the aeroelasticity analysis of multiple blade row configurations. It is found that a fully coupled multiple blade row model yields higher accuracy in predicting the flow behaviour of the turbomachines than the simplified isolated one [46]. This has motivated the authors to approach differently by considering wind turbines in arrays as a multi-stage turbine so that the frequency domain method can be applied to perform the rotor-stator interactions and the aerodynamic simulations of multiple turbines at an affordable computational cost.

It is clear from this above literature review that, while high-fidelity CFD simulations of the multiple wind turbines are important, the conventional time domain solution methods are impossible or difficult to be performed due to the high computational demand. On the other hand, it was revealed that frequency domain solution methods can provide accurate results with significantly lower computational cost compared to conventional time solution methods. Therefore, a novel nonlinear frequency domain solution method is proposed to model and study wind turbine in arrays in this study. In this paper, wind turbines in arrays will be modelled in multi-row configurations and the distance between the upstream turbine and the downstream one will be varied. The considered distances between the turbines are 2D, 5D and 10D, where *D* is the rotor diameter, and the effects of the upstream wind turbine on the downstream one will be investigated. This is the first time that a frequency domain method is applied to the investigation of multiple wind turbines. The main distinctive feature of this paper is the modelling of wind turbines in arrays as a multi-stage turbine and the application of the frequency domain solution method, which reduces the computation time significantly to a reasonable and affordable level.

2. PHYSICAL DESCRIPTION

Figure 1 shows the schematic view of two wind turbines in arrays with different distances in the present study. The MEXICO (Model Rotor Experiments In Controlled Conditions)

Experiment wind turbine model was experimentally tested and studied in a wind tunnel in the Large-Scale Low-Speed Facility of the German-Dutch Wind Tunnel (DNW) [7-10]. There are various numerical studies which have been conducted using this wind turbine model [47-50]. In this paper, the MEXICO-Experiment wind turbine model is modified to model the wind turbines in arrays by adding another rotor behind the first wind turbine. Each wind turbine has three blades, and the blade is 2.04 m long. The rotor diameter, *D*, is 4.5 m. The separation distance between the turbines in the axial direction (*W*) is defined in terms of rotor diameter, *D*, and the considered distances between the turbines are 2D, 5D and 10D in this study. To evaluate the effects of wind turbines in arrays on the flow behaviour and to analyse the aerodynamic performances of the wind turbines, the design condition from the experiment which corresponds to the wind speed of 15 m/s, the rotational speed of 424.5 RPM and the design pitch angle of -2.3 degrees are used in this study. Both upstream and downstream wind turbines are kept at the same rotational speed.

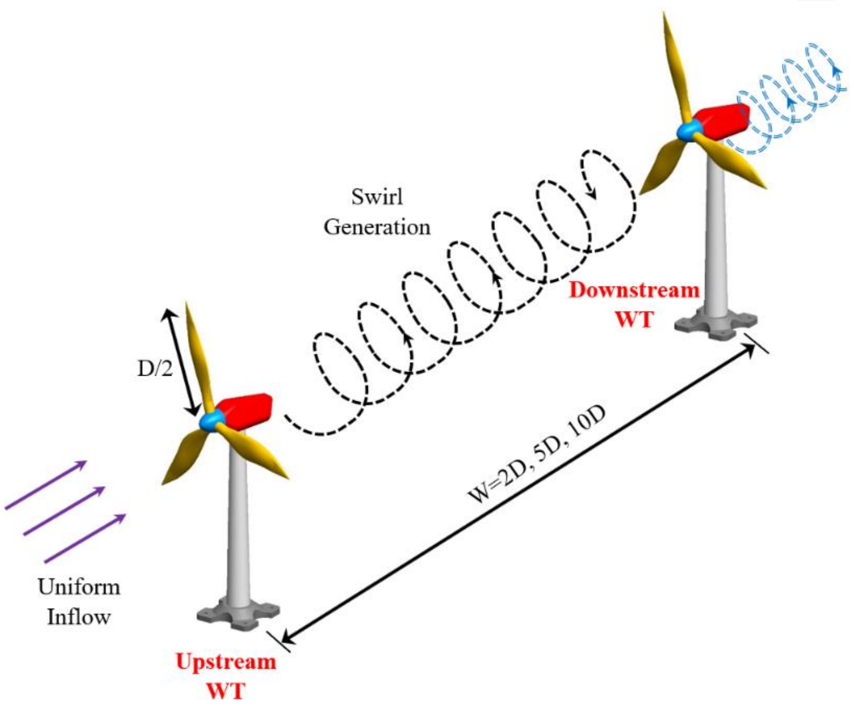

Figure 1. Schematic view of the two wind turbines in arrays with different separation distances

3. NUMERICAL METHODOLOGY

3.1. Computational Method

3.1.1. Governing Equations

In the present work, a three-dimensional density-based finite volume solver is employed for the flow computation. The simulations are performed based on the URANS model. The flow is governed by the Navier-Stokes equations and it can be expressed as:

$$\frac{\partial}{\partial t}\int_{\Omega} U d\Omega + \int_{S} \vec{F}_I \,. d\vec{S} + \int_{S} \vec{F}_V \,. d\vec{S} = \int_{\Omega} S_T d\Omega \tag{1}$$

where Ω is the volume, S is the surface, U is the vector of the conservative variables, S_T is the source term, and $\vec{F}_I$ and $\vec{F}_V$ are the inviscid and viscous flux vectors, respectively. Spalart–Allmaras turbulence model is employed in this work and the above equation can be simply written in a semi-discrete form as [43-46]:

$$\frac{\partial}{\partial t}(U) = R(U) \tag{2}$$

where R is the lumped residual and the source term.

3.1.2. Frequency Domain Solution Method

In this study, the sources of the flow unsteadiness are associated with the flow interaction in the multiple row configurations (i.e., the interaction between the rotor, tower (stator) and rotor). The unsteady terms corresponding to the flow unsteadiness can be represented by a Fourier series for a prescribed fundamental frequency, ω, and the specified number of harmonics, m, as expressed in Eq. (3).

$$U = \overline{U} + \sum_{m=1}^{M}[U_A \sin(m\omega t) + U_B \cos(m\omega t)] \tag{3}$$

where $\overline{U}$, U_A, and U_B are the Fourier coefficients of the conservative variables. The accuracy of the unsteady solution can be controlled through the order of the Fourier series. In this paper, as the source of flow unsteadiness is related to the flow interaction between the rotor and the tower which is periodic in time, the fundamental mode (one harmonic) is considered enough to resolve the flow. The blade passing frequency is the fundamental frequency of the system. Substituting Eq. (3) into Eq. (2) yields the following equations.

$$\omega \sum_{m=1}^{M}[mU_A \cos(m\omega t) - mU_B \sin(m\omega t)] = R \tag{4}$$

These new set of unsteady Navier-Stokes equations are solved in the frequency domain with the frequency domain method. With this method, the unsteady period for one complete rotor rotation is equally divided into $N = (2m+1)$ time levels and the system of nonlinear equations coupling all N time levels are then solved iteratively. After completion of the flow simulation, the frequency domain solution can be reconstructed in time to have a flow solution in time history, which can be directly compared to the time domains solution. A central scheme is used for the spatial discretization and a four-stage explicit Runge–Kutta scheme is used for the temporal discretization. Detailed formulation and implementation of the frequency domain solution method can be found in [43-46].

3.1.3. Rotor-Stator Interaction

The relative motion between successive rows of rotating and stationary domains such as rotor and tower is the main source of flow unsteadiness that affects the flow around the wind turbines in arrays. In this study, a rotor-stator interface is employed to exchange the flow solution between the rotating domain which includes a rotor and the stationary domain which includes a tower. The task of the rotor-stator interface is to match the flow solution between the upstream and downstream sides and to ensure the continuity of the unsteady flow across the interface.

The rotor-stator interface must be defined in the mesh generator after the mesh for each domain has been generated. The boundaries from the upstream domain and the downstream domain are connected using a full non-matching interface type, which allows to connect the grids with several blocks with non-matching boundaries. It means that the grid boundaries with different pitch lengths (i.e., rotational periodicity) can be connected. After connecting all grids together and defining the rotor-stator interface, a single grid file is imported into the flow solver where the rotor-stator interaction is set up, which indicates the flow direction, typically from the upstream to downstream direction. But the flow interaction between the rotor and stator is taken into account by transferring and exchanging the flow data between the two domains.

The standard sliding-plane method which is a time-accurate solution is applied for the time domain solution. In this method, by using a direct local interpolation method, the instantaneous flow information is exchanged across the interface at each time step. This method requires the same rotational periodicity on both sides, which means a full wheel of the rotor and the stator (both 360-degree grids) are required.

With a frequency domain solution method, on the other hand, the conservative flow variables can be decomposed into a time-averaged value and unsteady perturbations for a specified m harmonics, based on Fourier decomposition of the unsteady flow as expressed in Eq. (3). The equality of rotational periodicity is obtained through the phase-shift periodicity as the harmonic components are phase-shifted between periodic boundaries as explained in the next section.

Hence, the interaction between the rotor and the stator (i.e., the tower in this study) can be modelled by computing the time-averaged flow and the unsteady perturbations from the two adjacent rows and transferring the flow characteristics between the upstream row and the downstream row to ensure the continuity of the unsteady flow across the rotor-stator interface. The resolution and the continuity of the flow can be controlled through the order of Fourier series or the number of harmonics. More details of rotor-stator interface treatments can be seen in [36,37] and the applications of rotor-stator interfaces in the analysis of multi-stage turbines can be found in [45,46]. The schematic view of the rotor-stator interaction is shown in Fig. 2.

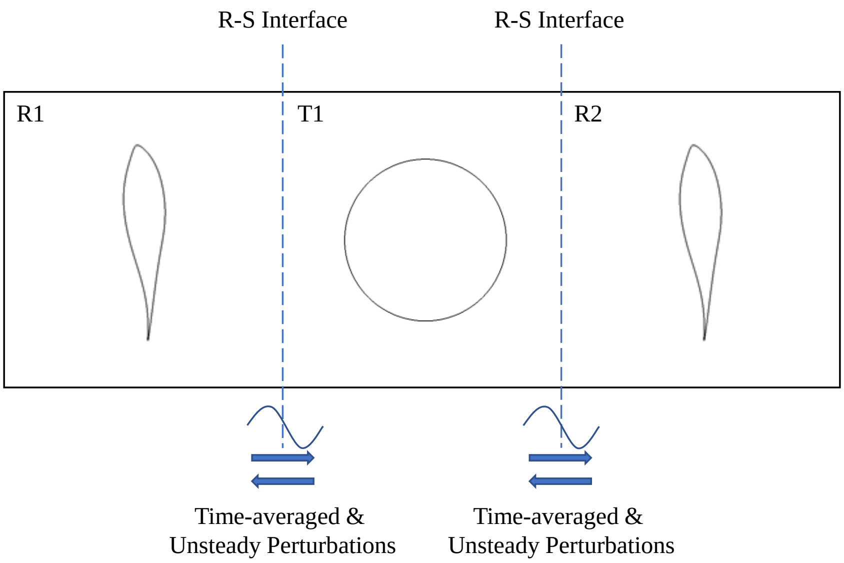

Figure 2. Schematic diagram of the rotor-stator interaction between the wind turbines in arrays. *(R1: Rotor of the upstream wind turbine; T1: Tower of the upstream wind turbine; R2: Rotor of the downstream wind turbine)*

3.2. Boundary Conditions

The solid wall boundary condition is applied on the blade, the hub and the tower. The external boundary condition, which is a non-periodic one, is defined to treat the far-field boundaries dealing with the external flow computations. A rotor-stator interface is used to connect the outflow surface of the rotor domain of the first wind turbine and the inflow surface of the tower domain of the first wind turbine. The same interface type is used to connect the outflow surface of the tower domain of the first wind turbine and the inflow surface of the rotor domain of the second wind turbine. For the periodic boundaries of the rotor, the direct periodic (repeating) condition is applied for the time domain method whereas only a single passage domain is required for the frequency domain solution method. With the frequency domain method, the harmonic components are phase-shifted between the periodic boundaries by a given Inter Blade Phase Angle (IBPA), σ, defined by the number of blades available in a rotor, and it is expressed in the following equations where the subscript 1 and 2 are corresponding to the referenced passage and its neighbouring one, respectively [43-46].

$$U_{A,2} = U_{A,1} \cos(\sigma) - U_{B,1} \sin(\sigma) \quad (5.a)$$

$$U_{B,2} = U_{A,1} \sin(\sigma) + U_{B,1} \cos(\sigma) \quad (5.b)$$

3.3. Computational Domain and Grid Generation

A new type of modelling method to simulate multiple wind turbines is proposed in this paper. Wind turbines in arrays can be modelled in a multiple-row configuration considering as a multi-stage turbine. In this study, there are two wind turbines in arrays, separated by a separation distance. In terms of modelling, ideally, there should be a rotor model and a tower model from each wind turbine. However, as this study investigates the effect of the upstream wind turbine on the aerodynamic performances of the blades of the downstream turbine, only the rotor model of the downstream turbine without the tower is included in the wind turbine in arrays model to reduce the computation time. However, using the proposed method, a series of turbines can further be modelled by adding more rotors and stators (i.e., towers). In order for the rotor-stator interface to work effectively for the flow continuation, all rotor blades and stator blades (i.e., tower in this model) have to be on the same hub. Therefore, an infinitely long hub is used in this paper to connect the rotors and the tower. An infinitely long hub was also employed in the simulation of wind turbines before [51] and it is assumed that the effect of the hub on the flow field around the wind turbines is not significant.

A structured grid generator is used to generate a three-dimensional computational domain and grid. In order to model wind turbines in arrays, the rotors and the tower are meshed separately, and they are connected through a rotor-stator interface. A Rounded Azimuthal O4H topology is used for the generation of both rotor and tower grids. Each grid consists of five blocks such as the skin block surrounding the blade, the inlet block located upstream of the leading edge, the outlet block located downstream of the trailing edge, the upper block located above the blade section, and the lower block located under the blade section. An O-mesh is used for the skin block whereas an H-mesh is used for the remaining blocks. The frequency domain solution method only requires modelling of a single passage or a single blade of a full rotor wheel, which is one of the main advantages of this method for the analysis of turbomachines with multiple blade rows. Using the frequency domain solution method, the harmonic components of the flow variables can be phase-shifted between periodic boundaries by a given an inter blade phase angle, as expressed in the boundary conditions section. Therefore, a 120-degree grid is only required for the rotor model for the frequency domain solution (see Fig. 3 (b)). On the other hand, the time domain solution method requires a full wheel of rotor and stator with all blades for the time-accurate solution. Figure 3 (a) shows the overall view of the computational domain including all three blades and tower. This is, in fact, the domain used for the time domain solution. A 360-degree grid is generated for the tower domain. The flow inlet and outlet are located 2D upstream of the rotor and 4D downstream of the rotor, respectively, and the far-field boundary is placed 1.5D from the origin of coordinates, where *D* is the rotor diameter. The first cell layer thickness is 1e-5 meters to ensure that the y+ value is less than one. The generated grid consists of 4.5 million grid points in each of the rotor domain with a single blade and 7.5 million grid points in the tower domain. Therefore, a total of 16.5 million grid points are required for the frequency domain solution whereas 34.5 million grid points are required for the time domain solution. The generated computational domain and the grid are shown in Fig. 3.

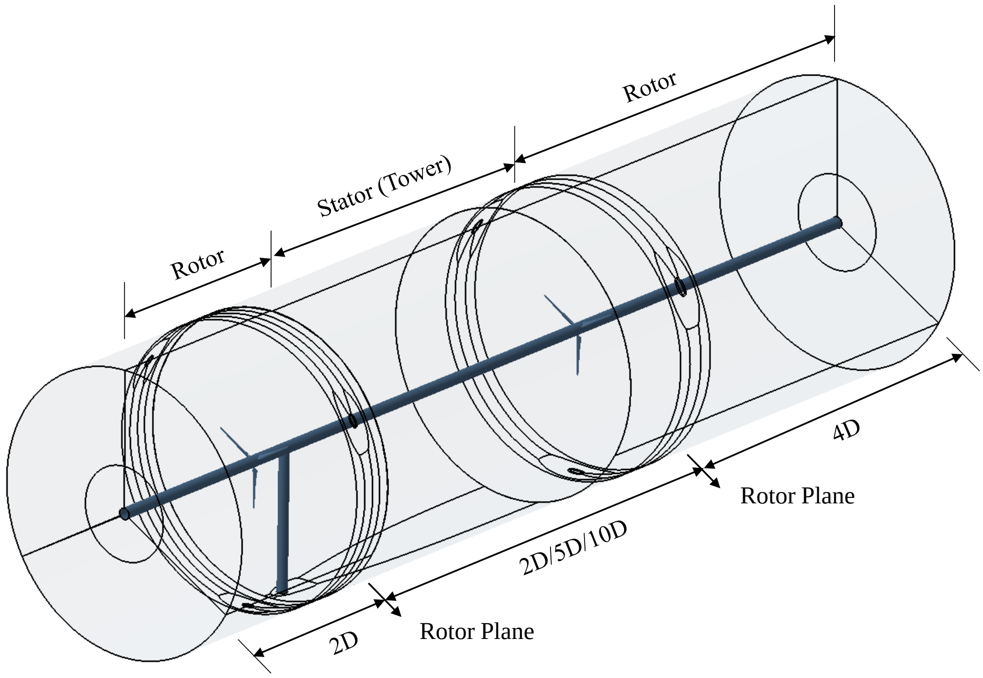

(a)

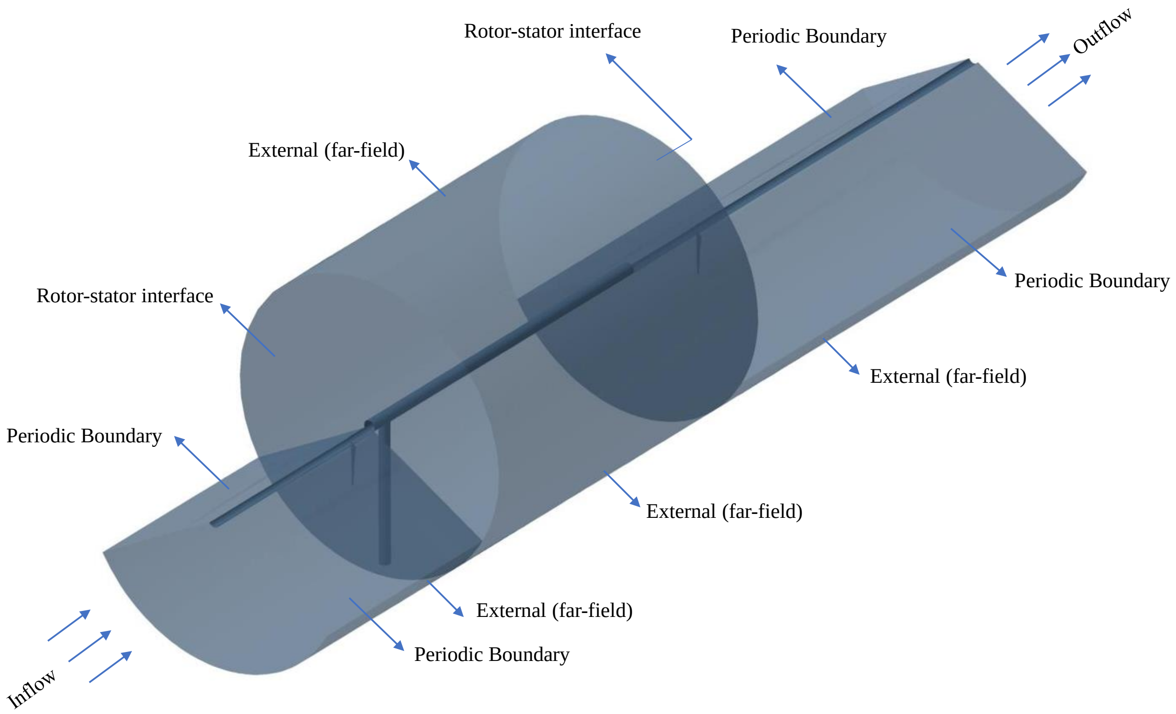

(b)

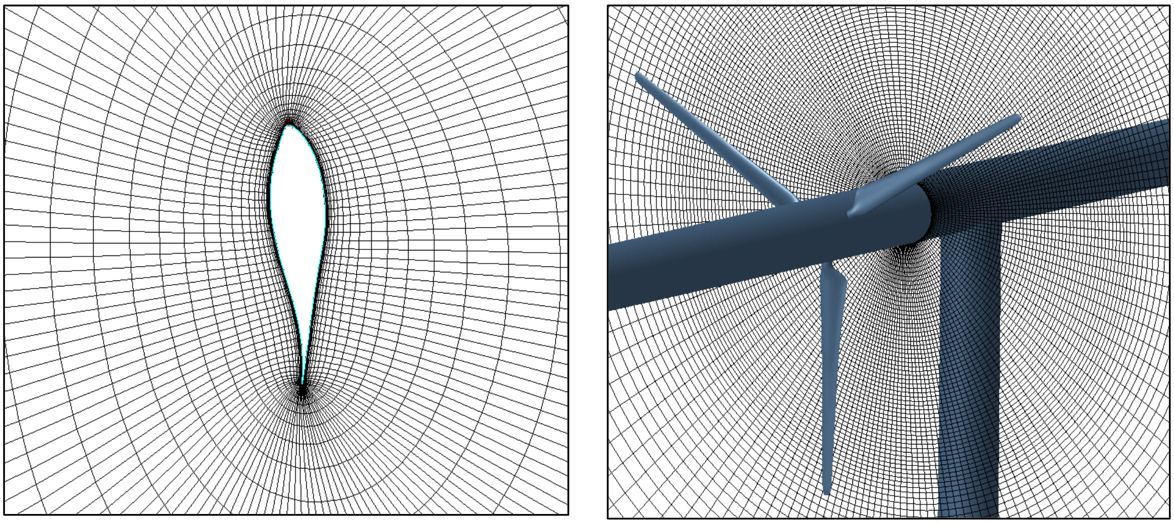

(c) (d)

Figure 3. The generated computational domain and grid: (a) Overall view of the computational domain, (b) details of boundary conditions, (c) blade-to-blade view of the mesh around the aerofoil and (d) rotor-stator interface.

4. VALIDATION

Before performing simulations of multiple wind turbines, it is essential to ensure the accuracy of the numerical model employed in this study. To this end, the simulation of a single wind turbine is first performed, and the pressure coefficients are compared to the experimental data and the numerical data of Sorensen et al. [47]. Figure 4 shows the steady pressure coefficient distributions on the surfaces of the blade obtained at 60% and 82% of the blade span sections. It can be seen that the present numerical results at different span sections are in good agreement with the experiment and the reference simulation. More details and comparison of pressure coefficients at other blade sections can be found in [43,44]. Therefore, the employed CFD model is accurate enough to predict pressure distributions on the blade surfaces.

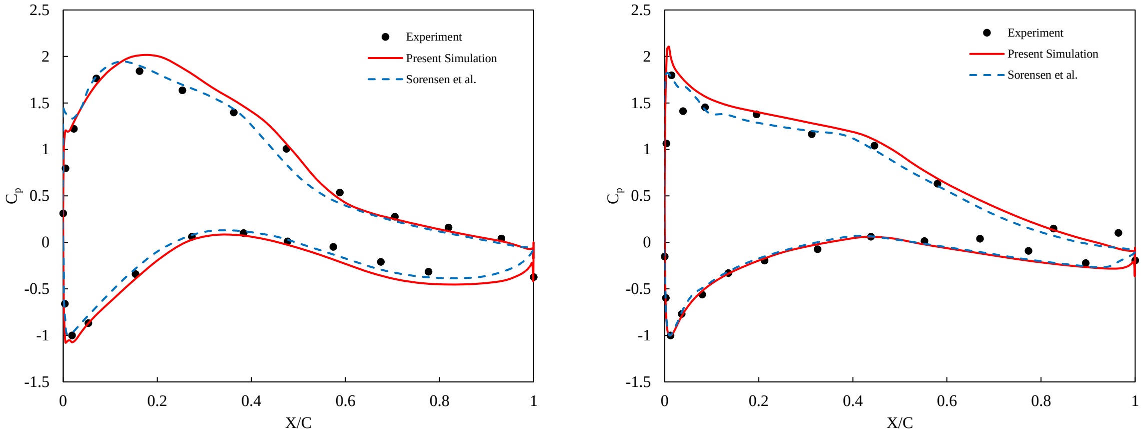

(a) (b)

Figure 4. Steady pressure coefficient distributions at (a) 60% and (b) 82% of the blade span obtained from the experiment, the reference simulation of Sorensen et al. [46] and the present simulation.

Figure 5 shows the comparison of the time-averaged pressure coefficient on the blade surfaces of the upstream wind turbine between the proposed frequency domain solution method and the time domain solution method based on the case in which the downstream wind turbine is placed at 2D behind the upstream wind turbine. The results are extracted at 25%, 30%, 50% 90% and 95% of the blade span sections. As seen, the results of the frequency domain method are in excellent agreement with the time domain method at different span sections.

Furthermore, Fig. 6 presents the variation of the time-averaged pressure coefficient on the blade surfaces of the downstream wind turbine at different span sections obtained from both time domain and frequency domain methods. Likewise, the results are obtained at different sections of the blade. As shown, the results from both methods are close to each other at all sections of the blade including 25% and 95% span sections, representing the bade root section and the tip section, respectively, where the flow is complex, which becomes problematic for the numerical methods. Therefore, it can be concluded that the frequency domain solution method accurately predicted pressure distributions on the surfaces of the blade of both upstream and downstream turbines. Contrary to the upstream turbine, significant deviations on the pressure distributions on the blade surfaces are observed at different sections, which is mainly due to the effect of the wake generated from the upstream wind turbine.

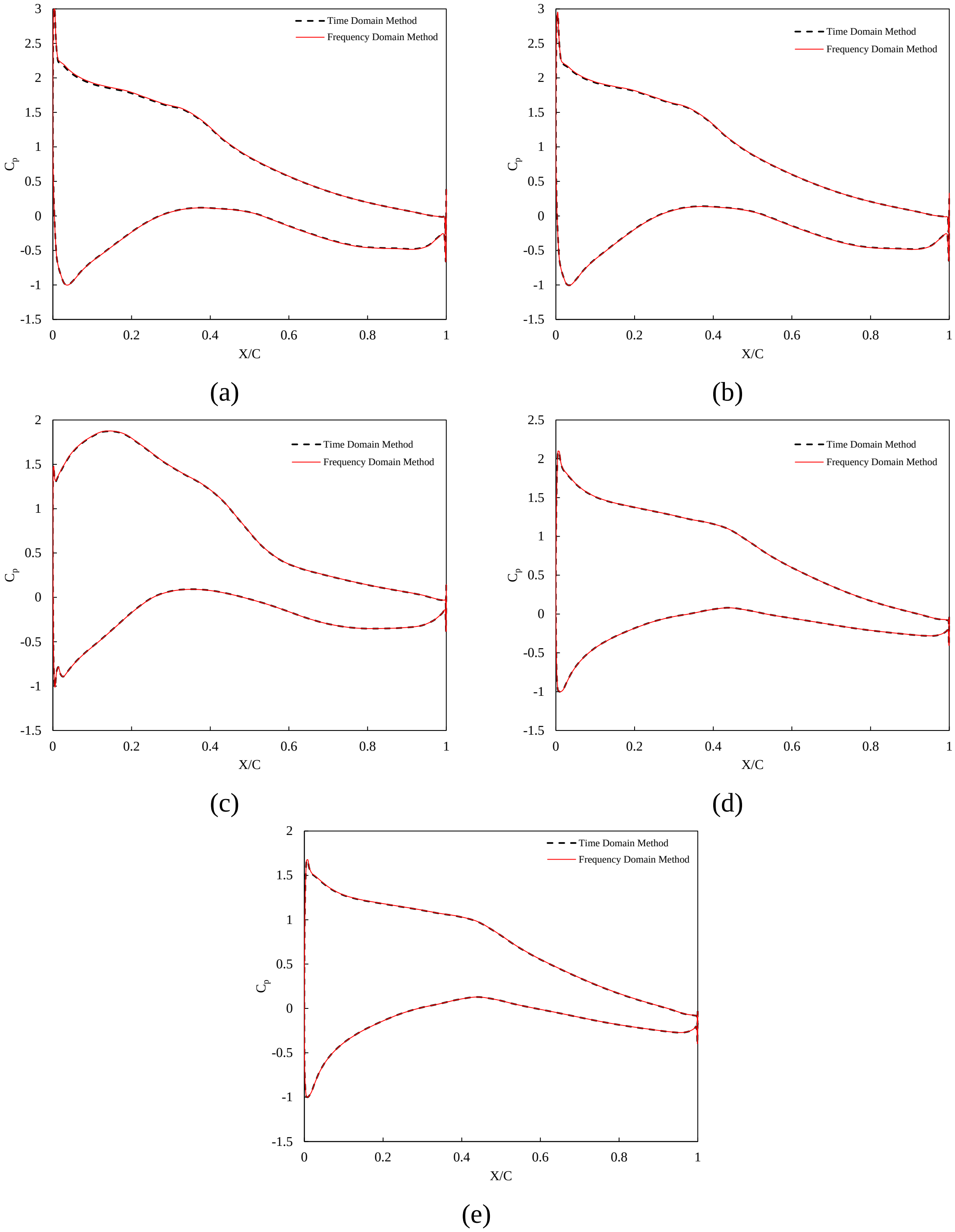

Figure 5. Time-averaged pressure coefficient distributions at (a) 25%, (b) 30%, (c) 50%, (d) 90% and (e) 95% of the blade span of the upstream wind turbine obtained from the time domain method and the frequency domain method.

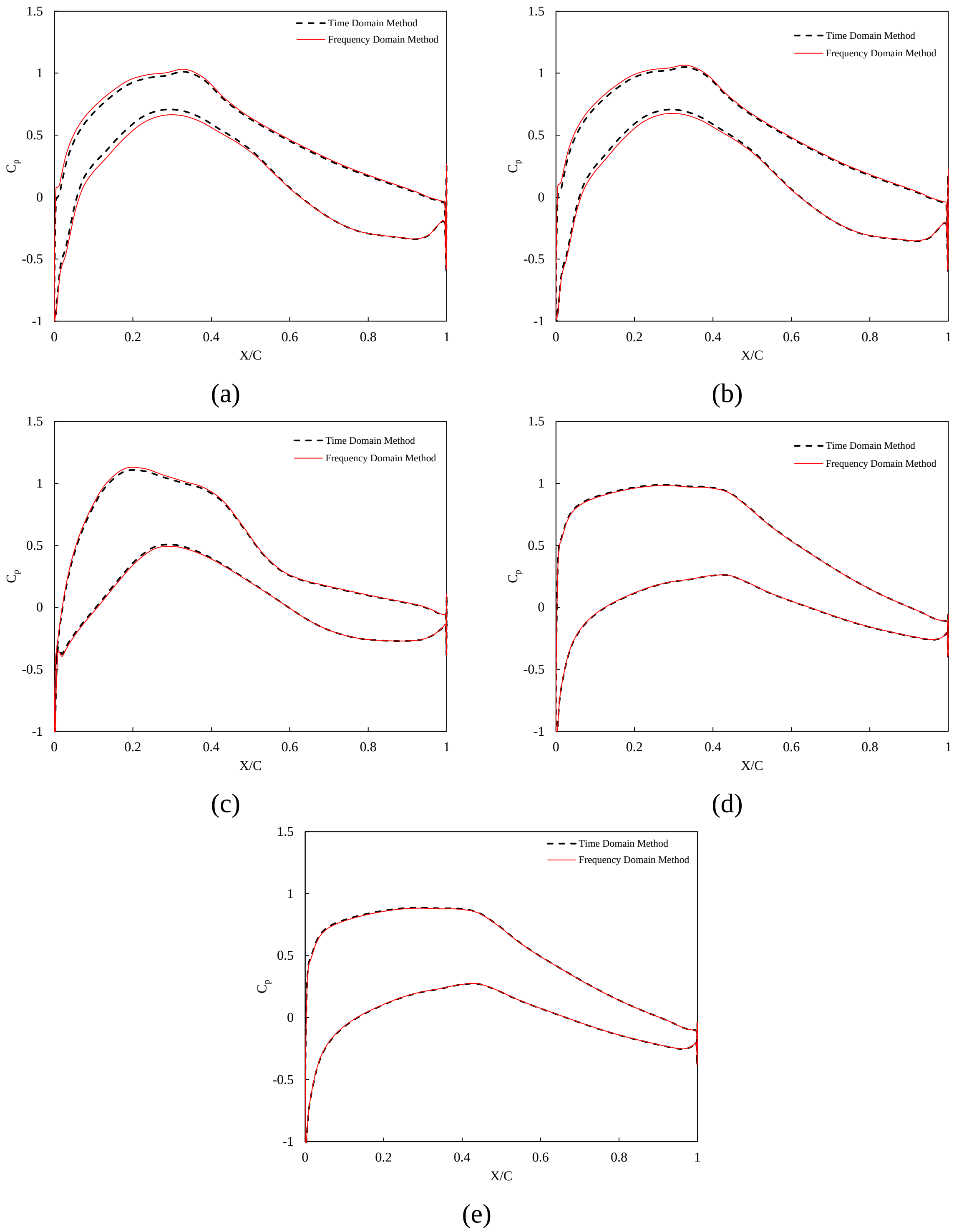

Figure 6. Time-averaged pressure coefficient distributions at (a) 25%, (b) 30%, (c) 50%, (d) 90% and (e) 95% of the blade span of the downstream wind turbine obtained from the time domain method and the frequency domain method.

The comparison between the time domain solution method and the frequency domain solution method on predicting the skin friction coefficient distributions on the blade surfaces of the upstream wind turbine and downstream wind turbine at the separation distance of 2D are presented in Figs. 7 and 8, respectively. Similar to pressure coefficients, the results are provided at different blade span sections, including 25%, 30%, 50%, 90% and 95% of the blade span. Likewise, the skin friction coefficients at different sections of the blade of both upstream and downstream wind turbines obtained from the frequency domain method are close to that of the typical time domain method. It is understood that the flow behaviours in the blade root region and the blade tip region are sometimes difficult to be accurately predicted by the numerical models due to the complex flow nature. However, it is seen that the results at all sections including 25% and 95% span sections obtained from both methods are in a good agreement, which indicates that the frequency domain method is accurate enough for the prediction of the aerodynamic parameters.

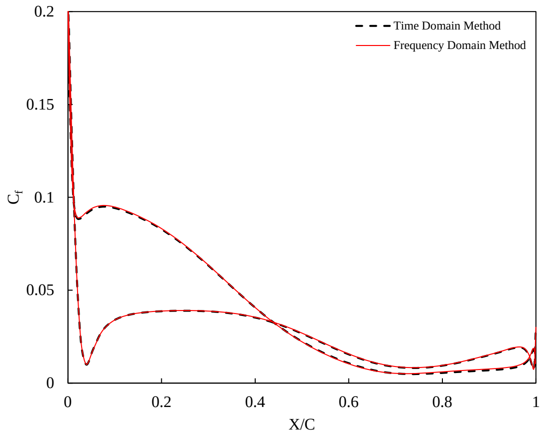

(a)

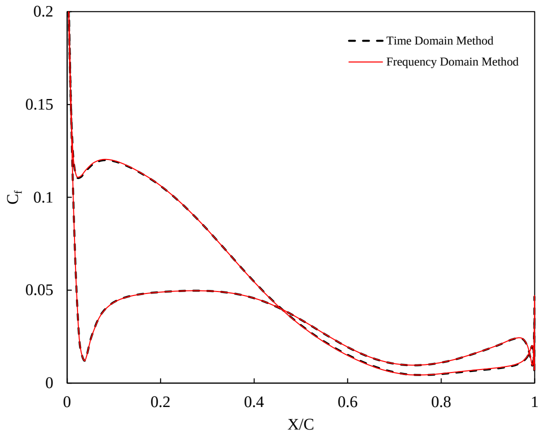

(b)

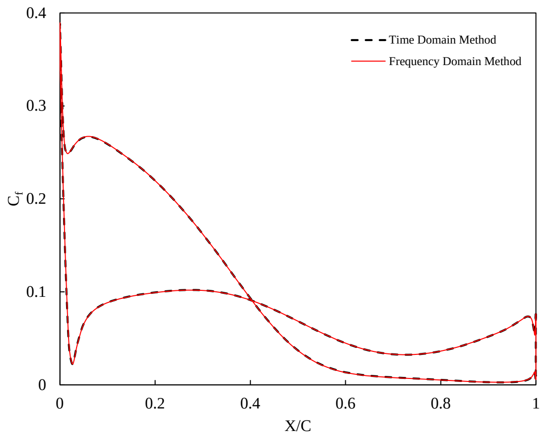

(c)

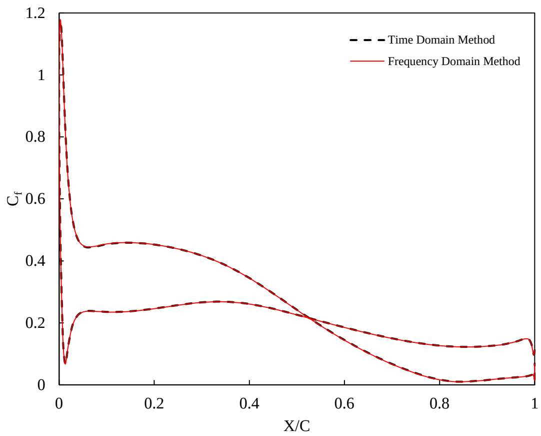

(d)

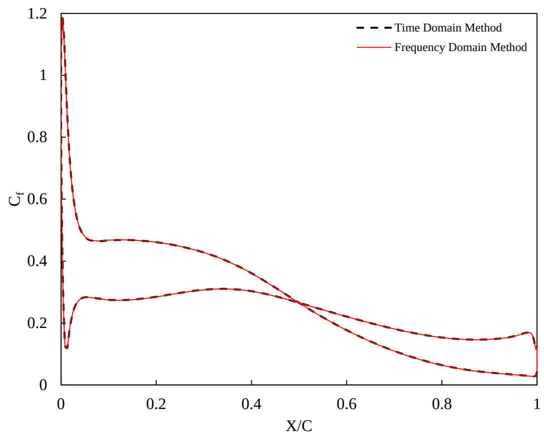

(e)

Figure 7. Skin friction coefficient distributions at (a) 25%, (b) 30%, (c) 50%, (d) 90% and (e) 95% of the blade span of the upstream wind turbine obtained from the time domain method and the frequency domain method.

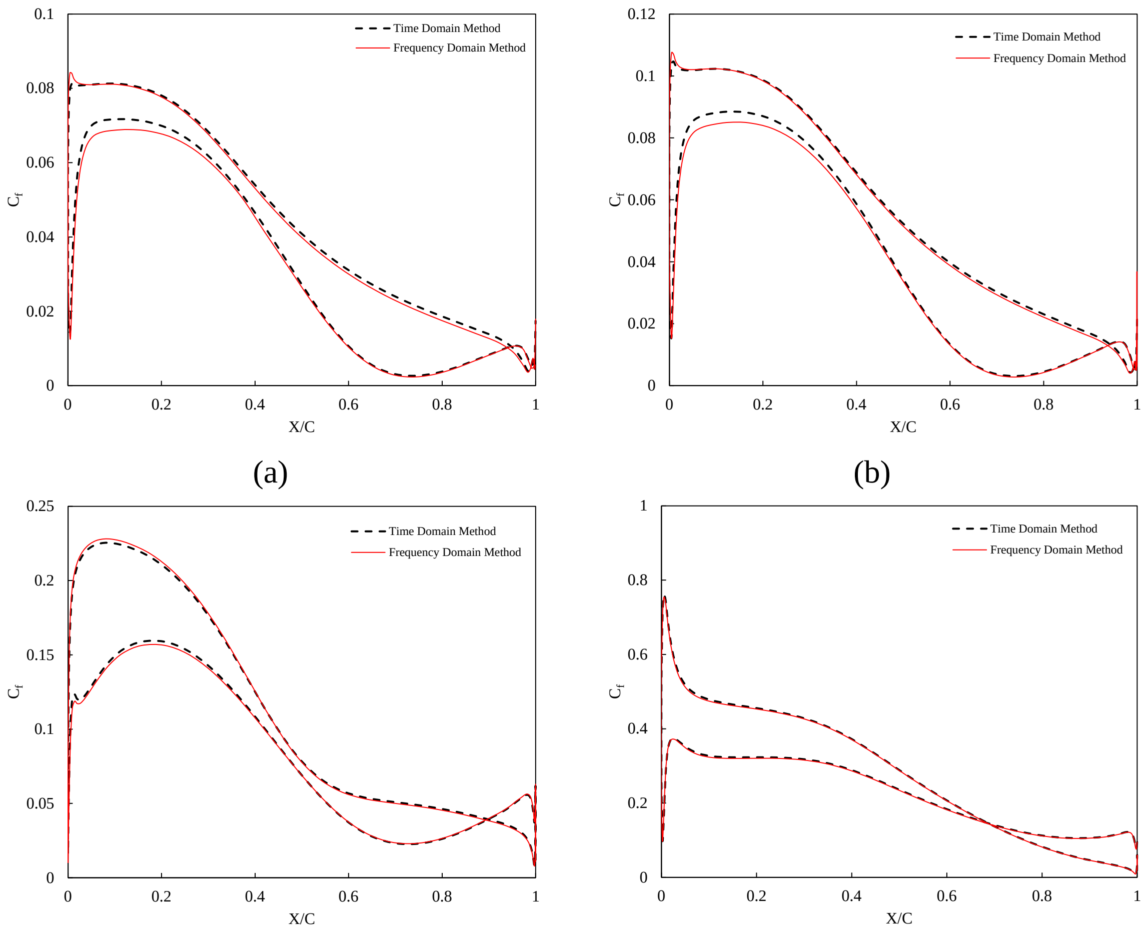

(a) (b)

(c) (d)

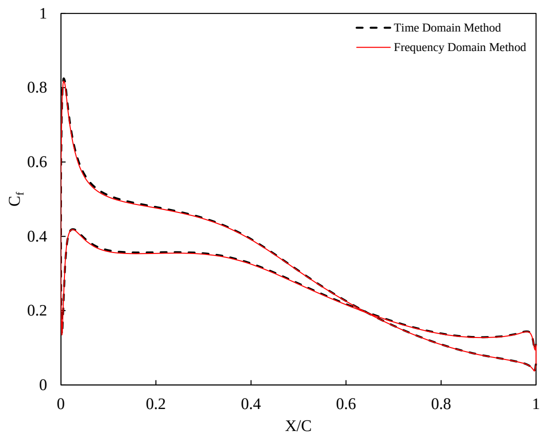

(e)

Figure 8. Skin friction coefficient distributions at (a) 25%, (b) 30%, (c) 50%, (d) 90% and (e) 95% of the blade span of the downstream wind turbine obtained from the time domain method and the frequency domain method.

Figure 9 demonstrates the comparison between the frequency domain method and the time domain method for the dimensionless wake profile extracted at 1D before the downstream wind turbine, on the horizontal plane at the blade mid-span section. The wake profiles are shown for a distance of 1D to each side from the rotor centre. Slight deviations are observed between the two methods; however, the differences are very small, and the results obtained are in good agreement. The wake profile is calculated based on the variations of the velocity magnitude over the reference inflow velocity (V/V_{ref}). It is seen that the lowest peak of the wake occurs near the X/D=0, which is at the rotor centre, and it has a symmetrical profile on both sides. Consequently, it can be deduced that the numerical model employed in the present study is able to capture the unsteady flow and predict the wake accurately. This also indicates that the flow variables are exchanged correctly at the interface between the rotating and stationary domains.

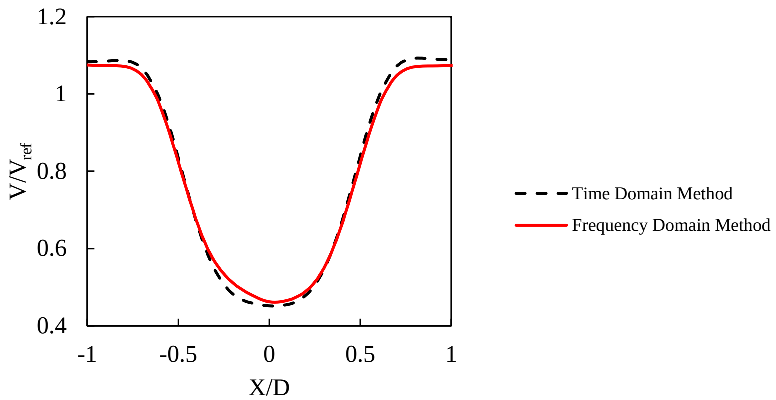

Figure 9. Wake profiles extracted at one rotor diameter before the downstream wind turbine obtained from the time domain method and the frequency domain method.

In-depth discussions on the effect of the upstream wind turbine on the downstream one will be presented in the next section. The results show that not only the proposed frequency domain solution method can capture the unsteady flow and calculate flow parameters accurately but also the rotor-stator interface has been applied correctly as the results are in close agreement between the two methods for both wind turbines. In order to highlight the advantage and the capability of the frequency domain method and also for a direct comparison between the two methods, the computational costs are compared for a period of an unsteady solution on a single CPU with a 3.40 GHz Intel (R) Core (TM) i5-7500 CPU. For the time domain solution, both a dual time-stepping method and a time-consistent multigrid method are employed for an effective and efficient computation. It has been proved that these methods can accelerate the computation. The simulation using the frequency domain method takes 6 hours whereas that of the time domain method takes 200 hours even with an efficient computation. The required numbers of period for an unsteady solution depends on the rotational speed and the distance between the two turbines. However, with a frequency domain solution method, the unsteady perturbations are computed based a period of the unsteady flow and the solution can be reconstructed in time to have the flow solution in time history. Therefore, the computational efficiency of the proposed frequency domain solution technique is considerable even when using a single CPU, and simulations of multiple wind turbines can be performed efficiently with this method. Therefore, it is concluded that the frequency domain solution method can be reliably utilised for further simulations of wind turbines in arrays by varying the distance between the two turbines.

5. RESULTS AND DISCUSSIONS

Figure 10 compares the time-averaged pressure coefficients obtained from the upstream wind turbine and the downstream wind turbine using different separation distances. The black line represents the pressure coefficient from the rotor blades of the upstream wind turbine whereas the rest of them are from that of the downstream wind turbine at different separation distances. The effect of the wake from the upstream wind turbine on the downstream one can be seen at all distances. The impact is much higher and more significant at the separation distances of 2D and 5D. This indicates that the separation distance of 5D is not far enough for the downstream wind turbine to avoid pressure losses if the downstream wind turbine is to be placed in the wake region of the upstream one. The flow recovers beyond the distance of 5D and the downstream wind turbine is less affected by the upstream one at 10D distance. However, there is still a noticeable impact from the upstream wind turbine even at this far distance. The results illustrate that the pressure coefficient on the blade surfaces of the downstream turbine at X/C=0.2 is increased by approximately 30% by raising the distance from 2D to 10D at 50% span. Strong deviations in pressure distributions are detected near the leading edge of the blades whereas a similar trend is noticed after X/C=0.5. These deviations are mainly caused by the non-uniform inflow with lower velocity magnitude which alters pressure distributions near the leading edge. This effect becomes much smaller at 10D distance where the flow is nearly uniform again. These observations indicate that the effect of the upstream wind turbine can be reduced by raising the distance from 5D to avoid significant pressure losses for the downstream wind turbine.

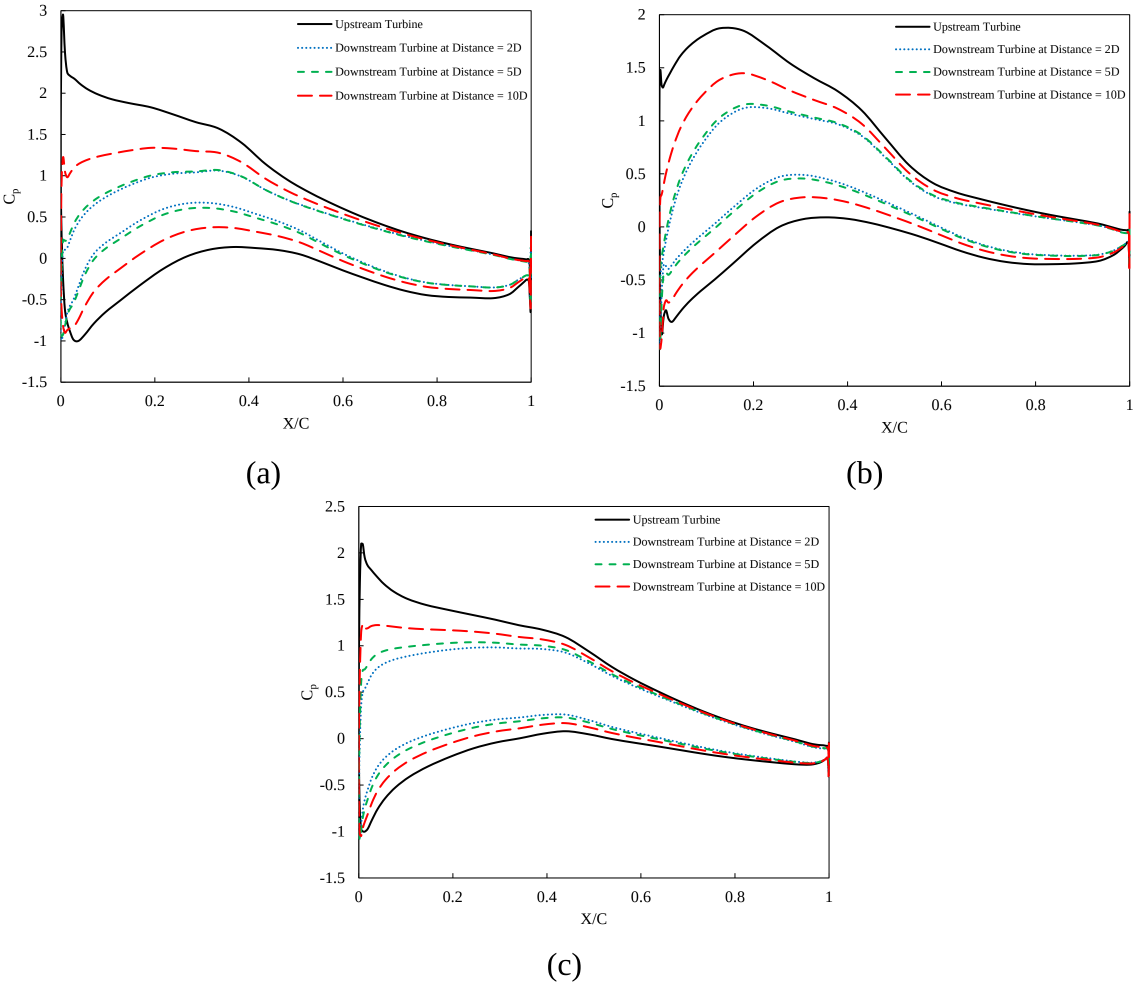

Figure 10. Time-averaged pressure coefficient distributions at (a) 30%, (b) 50% and (c) 90% of the blade span of the upstream wind turbine and the downstream wind turbines at different separation distances.

Unsteady pressure distributions on the blade surfaces of both upstream and downstream wind turbines can be visualised in Figs. 11-12. Unsteady pressure distribution can be decomposed into the time-averaged value and amplitude of unsteady fluctuations as expressed in:

$$P = \bar{P} + P_A sin\,(\omega t) + P_B \cos\,(\omega t) \quad (6)$$

where $\bar{P}$ is the time-averaged pressure and P_A and P_B are Fourier coefficients. Unsteady pressure amplitude can be defined as: $\tilde{P} = \sqrt{{P_A}^2 + {P_B}^2}$. Figure 11 presents the time-averaged pressure contour on the pressure and suction surfaces of both wind turbines. On the blade of the upstream wind turbine, higher pressure distributions are seen on the pressure surface near the leading edge and the trailing edge whereas lower pressure distributions are observed on the suction surface from approximately 40% of the blade span. In the case of downstream wind turbines, pressure distributions on the blade surfaces are lower due to the wake of the upstream wind turbine. At the separation distances of 2D and 5D, the pressure is higher near the trailing edge than the leading edge. Lower pressure field is developed within 60% - 100% of the blade span sections on the suction surface, which is shorter than that of the upstream wind turbine. In the case of 10D separation distance, the pressure seems to recover as it is far away from the upstream wind turbine. On the pressure surface, the pressure is higher near both leading and trailing edges than that of the 2D and 5D cases whereas the low-pressure field starts to occur at approximately 55% of the blade span section, which is closer to that of the upstream wind turbine. However, the effect of the upstream wind turbine is still present by the noticeable amount even at this far distance as pressure distributions on the blade surfaces of the downstream wind turbine are lower.

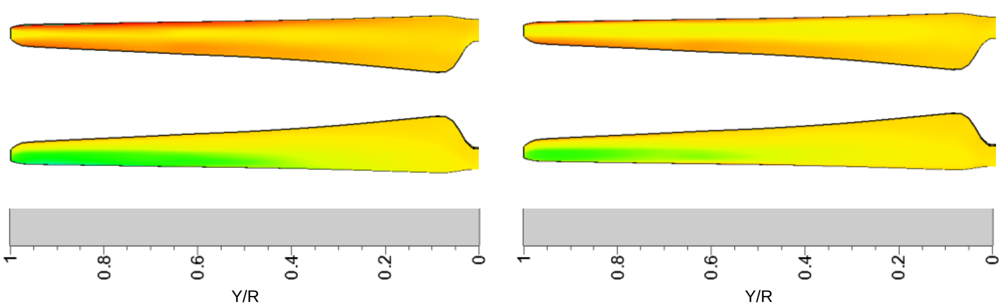

(a) (b)

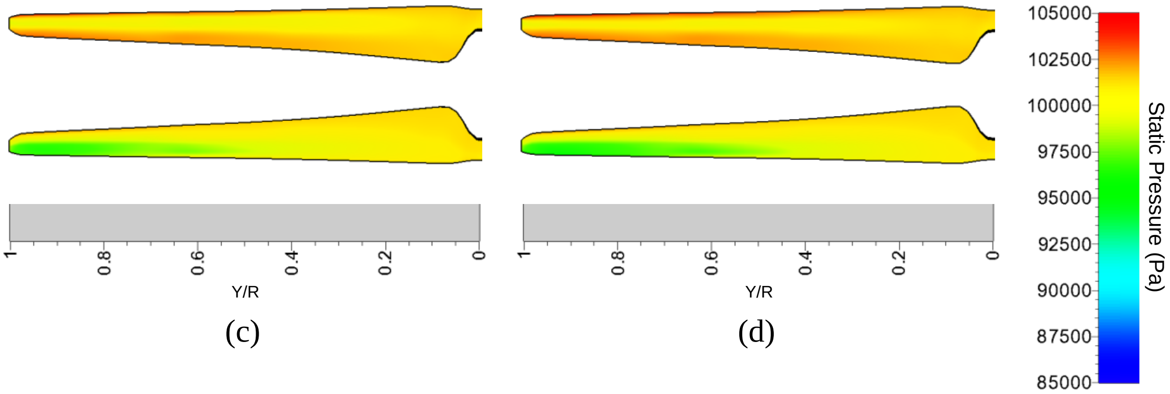

Figure 11. Time-averaged pressure ($\bar{P}$) distributions on the pressure surface *(upper)* and the suction surface *(lower)* of the blade from (a) the upstream wind turbine, (b) the downstream wind turbine at the separation distance of 2D (c) the downstream wind turbine at the separation distance of 5D and (d) the downstream wind turbine at the separation distance of 10D.

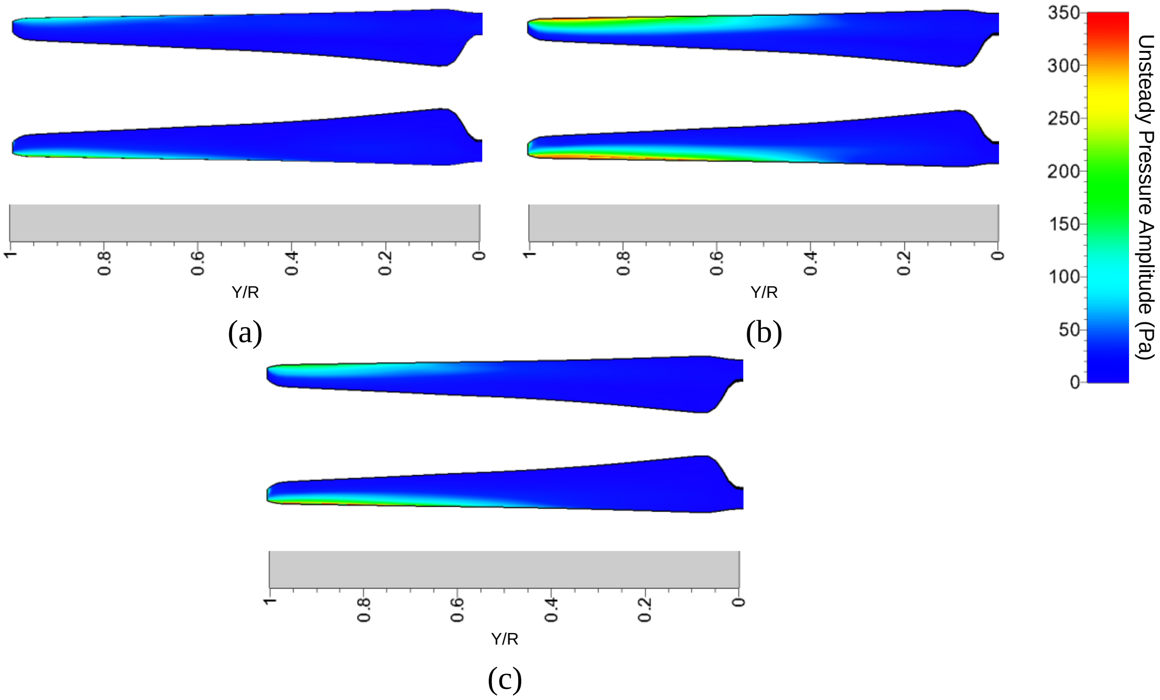

Figure 12. Unsteady pressure amplitude ($\tilde{P}$) distributions on the pressure surface *(upper)* and the suction surface *(lower)* of the blade from (a) the downstream wind turbine at the separation distance of 2D (b) the downstream wind turbine at the separation distance of 5D and (c) the downstream wind turbine at the separation distance of 10D.

Figure 12 depicts the unsteady pressure amplitude contours on the pressure and suction surfaces of the downstream wind turbine placed at different separation distances behind the upstream wind turbine. The amplitudes of unsteady fluctuations are only visible in the cases of the downstream turbine. At the separation distance of 2D, some unsteady pressure fluctuation is seen near the blade tip on both surfaces. However, compared to the 2D separation distance case, the amplitude of the unsteady pressure is much higher at 5D separation distance. Unsteady pressure distributions are also seen on both surfaces, around the leading edge, starting from approximately 40% of the blade span section. In the case of 10D separation distance, the unsteady pressure fluctuations tend to decrease as it is lower than that of the 5D separation distance case. However, the amplitude and fluctuations are still higher than the 2D separation distance case. These results and observations show that the far wake imposes more turbulence and flow disturbances, and it has more significant impact on the unsteady pressure distributions on the blade surfaces of the downstream wind turbine than the near wake as the amplitude is maximum at 5D separation distance and it tends to reduce beyond this distance.

Pressure distributions on the blade surfaces are directly related to the aerodynamic loads acting on the blade surfaces. The aerodynamic loads applied on the blade surfaces are provided in terms of torque and force profiles. The force profiles are evaluated based on the axial thrust. Figure 13 shows the torque and force coefficient profiles acting on the surfaces of the upstream wind turbine and downstream one at different separation distances. The coefficients, denoted by τ/τ_{max} for torque and F/F_{max} for force, are defined as: *(Torque on Blade-Average Torque on Blade)/(Maximum Torque on Blade)* and *(Force on Blade-Average Force on Blade)/(Maximum Force on Blade)*, respectively. Both torque and force profiles are plotted with respect to the transient dimensionless computation time for one complete rotor revolution. The results show that, in the case of the upstream wind turbine, the force profile is nearly uniform with some fluctuations whereas the deviation of the torque profile is noticeably stronger. However, harmonic force profiles are detected for both torque and force profiles on the blade of the downstream wind turbines. The amplitudes of the torque and force coefficients are intensified by 75% and 70%, respectively, when increasing the separation distance from 2D to 5D and then they tend to reduce by 20% and 50%, respectively, when increasing the distance between the wind turbines from 5D to 10D. It is noted that the difference in amplitude between the 5D and 10D cases is smaller for torque profiles than force profiles. In both cases, the aerodynamic loads acting on the blade surfaces are maximum at the 5D separation distance due to the flow turbulence and the far wake effect from the upstream wind turbine. These are consistent with the unsteady pressure distributions discussed in Fig. 12.

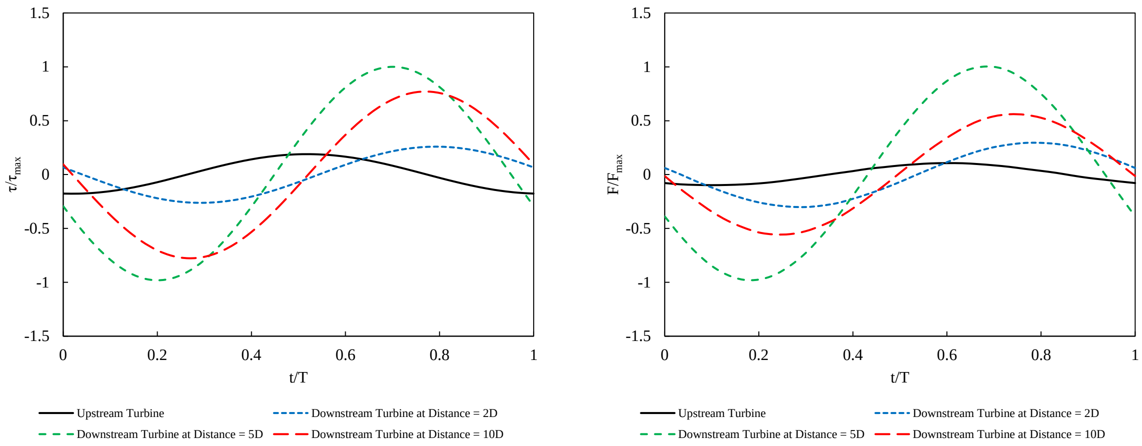

(a) (b)

Figure 13. (a) Torque profile and (b) force profile applied on the blade surfaces obtained from the upstream wind turbine and the downstream wind turbines at different separation distances.

Figure 14 demonstrates the comparison of the skin friction coefficients on the blade surfaces of the upstream wind turbine and the downstream one placed at different separation distances. Similar to pressure coefficient distributions, the skin friction coefficients on the blade surfaces of the downstream wind turbine are most affected by the upstream wind turbine at the separation distances of 2D and 5D. However, it is less affected at the separation distance of 10D as it is very far from the upstream wind turbine. At this distance, the wake generated from the upstream wind turbine recovers and the flow is nearly uniform again. This leads to a similar trend of skin friction coefficient distribution on the blade surfaces of the downstream wind turbine as that of the upstream turbine, but some noticeable variations and effects from the upstream turbine are still observed. The results show that the skin friction coefficient is the highest near the leading edge of the wind turbine blade due to the boundary-layer flow formation in this region. The fluctuations in the skin friction coefficient with respect to X/C are mainly related to the flow separation and recirculation over the suction surface of the blade.

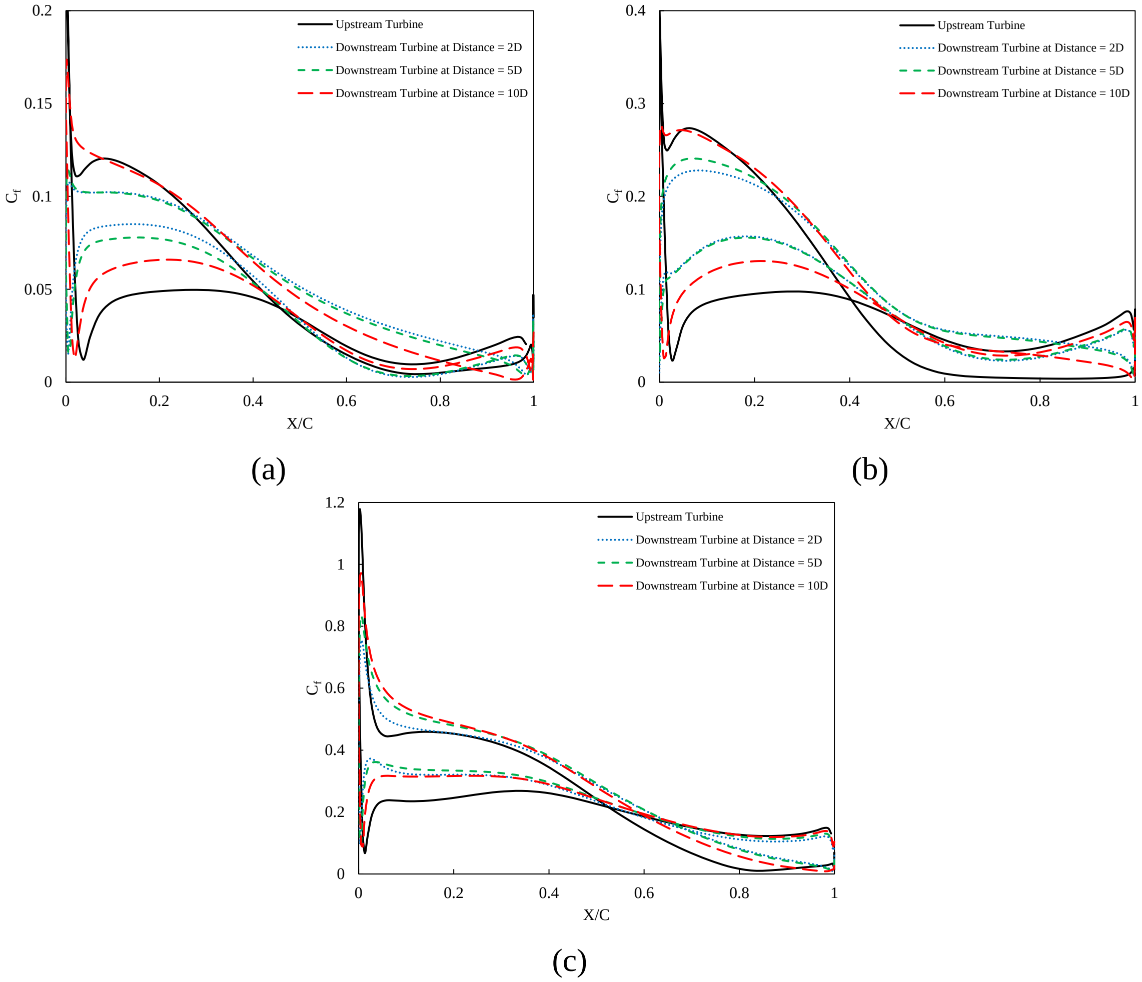

Figure 14. Skin friction coefficient distributions at (a) 30%, (b) 50% and (c) 90% of the blade span of the upstream wind turbine and the downstream wind turbines placed at different distances behind the upstream turbine.

Figure 15 illustrates the instantaneous velocity profiles or wake profiles calculated at 1D before the downstream wind turbine from each case with different separation distances. By plotting the instantaneous velocity profiles, the behaviour of flow in both space and time (i.e., the velocity magnitude at different locations at a certain physical time) can be determined. The profiles are extracted on the horizontal plane at the blade mid-span section for a distance of 1D to each side from the rotor centre. These profiles demonstrate the wake profiles with respect to the distance from the upstream wind turbine as well as the inflow profile for the downstream wind turbine. The -0.5X/D to 0.5X/D region lies within the rotation of the blades and the velocity in this region is reduced as the flow interacts with the blade which then captures the energy from the wind. The results show that the amplitude of the wake profile becomes smaller by increasing the distance from the upstream wind turbine. The minimum peak of the wake occurs around the rotor centre; however, it is shifted towards 0.09X/D at 9D behind the upstream wind turbine which is 1D before the downstream wind turbine at the separation distance of 10D. It was observed that the unsteady perturbations are maximum at the 5D separation distance, which is why a small shift in the profile is seen at 4D distance. It is also noted that the wake beyond 5D distance gradually recovers; however, the unsteady perturbations are still present with low intensity. Even at the distance of 10D which is far away from the first turbine, where the flow seems to be more uniform, the perturbations and swirl flow are not completely vanished. Furthermore, as a result of the recovery process from the unsteady fluctuations, the inflow profile for the downstream turbine is not aligned with the rotor. This is the reason why the minimum peak for the velocity profile at 9D distance shifts slightly towards the positive side. The fact that the wake profiles at 4D and 9D distances shift towards the positive side is related to the direction of the rotation of the rotor as both turbines rotate in the same direction with the same rotational speed. These profiles indicate that the wake from the upstream wind turbine is still significant at the distance of 4D behind the upstream turbine. Therefore, a great impact on flow parameters was seen on the blade of the downstream wind turbine placed up to 5D from the upstream turbine. However, at the distance of 9D, the amplitude of the wake profile reduces and the inflow velocity for the downstream wind turbine tends to be closer to the reference velocity.

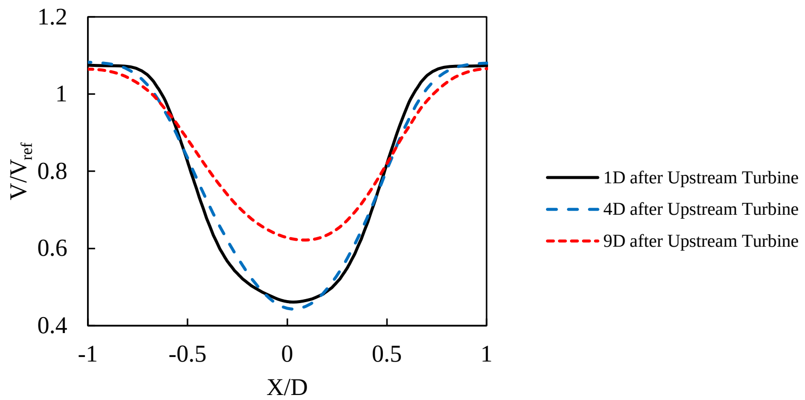

Figure 15. Wake profiles calculated at the distances of 1D, 4D and 9D behind the upstream wind turbine.

Figure 16 demonstrates the wake profiles 1D after both upstream and downstream wind turbines with different separation distances. The profiles are extracted in a similar way to the previous profiles. This figure compares the near wake profiles after the flow interaction with each turbine. Compared to the upstream wind turbine, the velocity drop in the region of the blade rotation (i.e., -0.5X/D to 0.5X/D) is more sudden and significant in the cases of the downstream wind turbine and some variations are also seen near the rotor centre. The amplitudes of the wake profiles at the distance of 1D behind the downstream turbine reduce by increasing the distance between the two turbines. Large separation distance reduces the impact on the downstream turbine, and the magnitude of the wake generated from the downstream turbine at the separation distance of 10D is closer to that of the upstream turbine compared to other cases. Furthermore, it is noted that the inflow is completely uniform and steady at a reference velocity for the upstream wind turbine whereas the profile is parabolic with lower magnitude but stronger velocity distribution in the blade tip region for the downstream wind turbine. The inflow profiles for each downstream turbine case can be understood looking at the profiles presented in Fig. 15. For instance, the profile at 9D distance is the inflow profile for the downstream turbine at 10D distance in Fig. 15. By increasing the separation distance to 10D, the intensity of the flow perturbation and recirculation are reduced, but their effects are still present. This is the main reason why the wake profiles at 1D behind the upstream wind turbine and the downstream wind turbine are not similar. The impact of the swirl flow produced by the upstream wind turbine on the downstream one is significant at the separation distance of 2D, and it is reduced by increasing the distance to 10D, but it is not vanished. The main reasons for obtaining different shapes of the wake profile can be explained in similar way. The recirculation and flow perturbations generated from the upstream wind turbine alongside the lower velocity magnitudes due to the wakes will have noticeable impact on the amplitude of the wake profiles of the downstream one. The flow structures become more non-uniform by reducing the distance between the wind turbines from 10D to 2D.

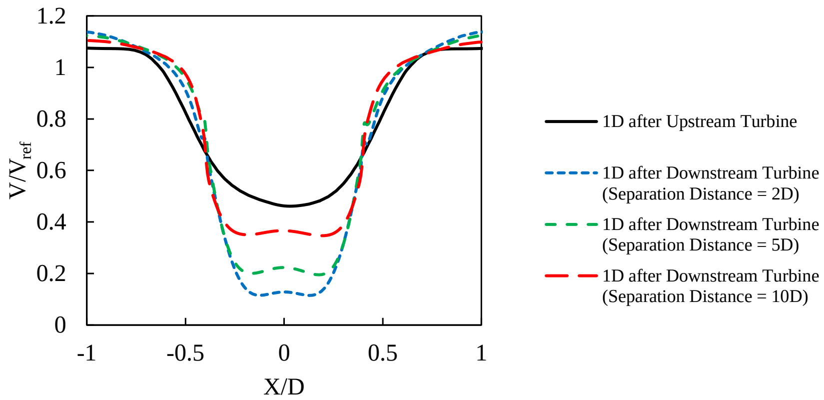

Figure 16. Wake profiles calculated at 1D after the upstream wind turbine and 1D after the downstream wind turbines at different separation distances.

The wake profiles, discussed in Fig. 16, can be better understood by looking at velocity contours extracted at 1D behind each turbine on the plane normal to the wind direction (See Figure 17). This figure particularly provides the flow information for visualisation of the flow condition at the same distance behind each turbine. It is seen that, in the case of the upstream wind turbine, the velocity distribution from the blade tip region to the blade root region is relatively linear whereas multiple layers of different velocity magnitudes are observed behind the rotors of downstream wind turbines. The velocity field is significantly affected after the flow interacts with the downstream wind turbine. The flow condition at the distance of 1D behind the downstream turbine depends on the separation distance. The velocity magnitude within the blade rotation, especially from approximately 40% to 80% span, is dramatically reduced when the downstream turbine is closer to the upstream turbine and it rises as the separation distance increases. Significant drops in the wake profiles, seen in Fig. 16, are associated with this physical phenomenon.

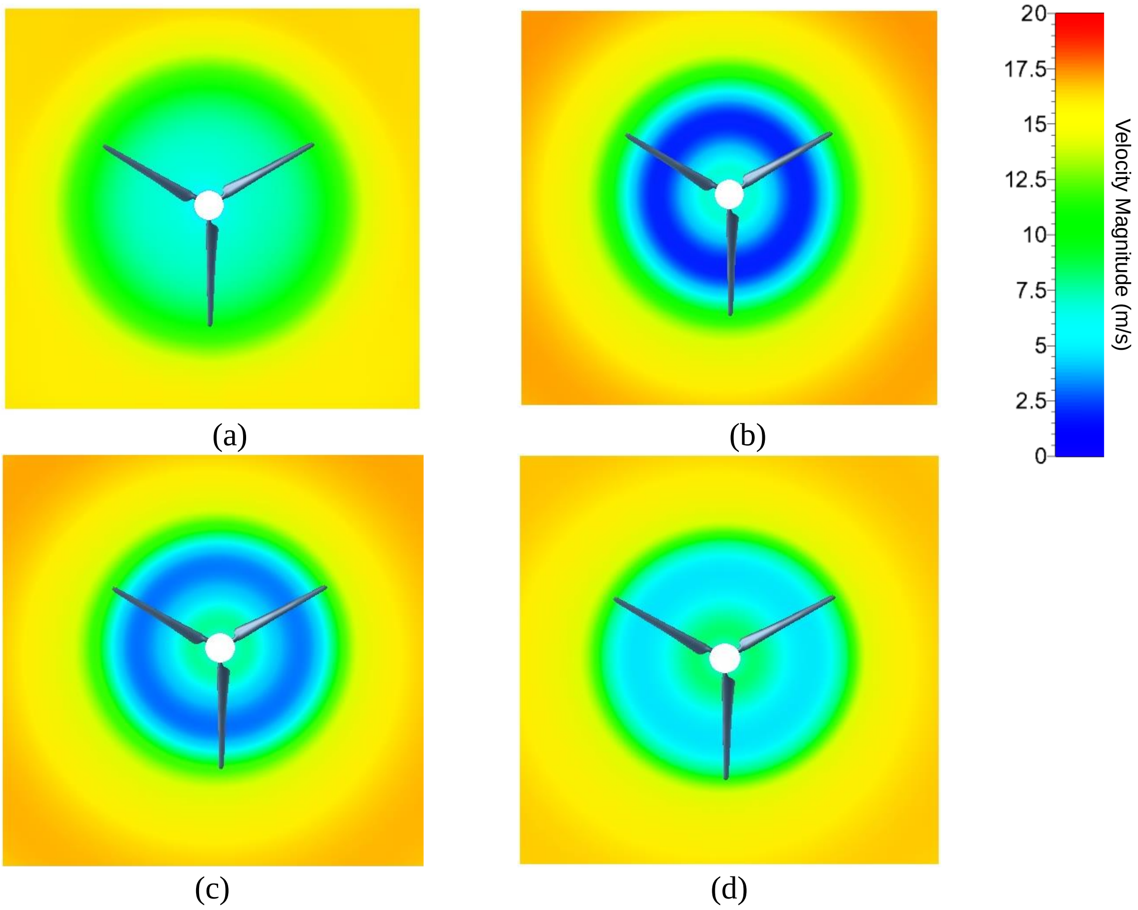

Figure 17. Velocity fields on the plane extracted at 1D behind (a) the upstream wind turbine, (b) the downstream wind turbine with the separation distance of 2D, (c) the downstream wind turbine with the separation distance of 5D and (d) the downstream wind turbine with the separation distance of 10D.

The instantaneous velocity contours in the meridional view from different separation distance cases are provided in Fig. 18 to visualise the flow field around and between the two wind turbines. The uniform inflow velocity is dramatically reduced after the flow interaction with the upstream wind turbine. In the case of 2D separation distance, the lower velocity field or the wake and the swirl flow generated from the upstream turbine are still strongly present at the distance of 2D behind the turbine where the downstream is located. As a result, the flow around the downstream turbine is most dominated by the wake of the upstream turbine at this distance and the velocity magnitude is further reduced behind the downstream turbine. In the case of 5D separation distance, the wake from the upstream turbine gradually reduces but its influence on the downstream turbine is still significant. However, at 10D separation distance, the lower velocity field resulted from the flow interaction with the upstream turbine shrinks as the wake recovers and the flow seems to be nearly uniform again. However, it should be noted that, as discussed in Fig. 16, the swirl flow and unsteady perturbations from the upstream turbine are still present at this distance. Despite the flow becoming more uniform at the 10D distance compared to other cases, it is not entirely uniform yet as the velocity profile is parabolic shape. It is seen that the magnitude of the inflow velocity is lower than the reference velocity; however, it is larger than any other cases. As a result, the trends of the distributions of flow parameters such as pressure on the blade surfaces on the downstream turbine are similar to that of the upstream turbine with less magnitude due to lower inflow velocity. Furthermore, it is also observed that the separation distance has an impact on the vortex generation and flow circulation from the tips of the blades of the downstream wind turbine. The size of the tip vortex structures around the downstream turbine at the separation distance of 2D is higher than any other cases as it combines with those from the upstream turbine due to small separation distance. As the separation distance increases, the vortex structures generated from the blades of the upstream turbine continue to a certain distance before gradually losing its intensity, but it is too far to reach the downstream turbine if the turbine is placed at 10D distance. As the inflow for the downstream wind turbine is not uniform and identical as it is for the upstream one, the wake behind the downstream turbine involves more turbulence and unsteadiness. The flow recirculation generated from the upstream wind turbine also has an impact on the flow disturbance and boundary-layer disruption near the blades of the downstream rotor. The flow unsteadiness and the influences of the wakes on the flow field around the wind turbines are considerable at different separation distances.

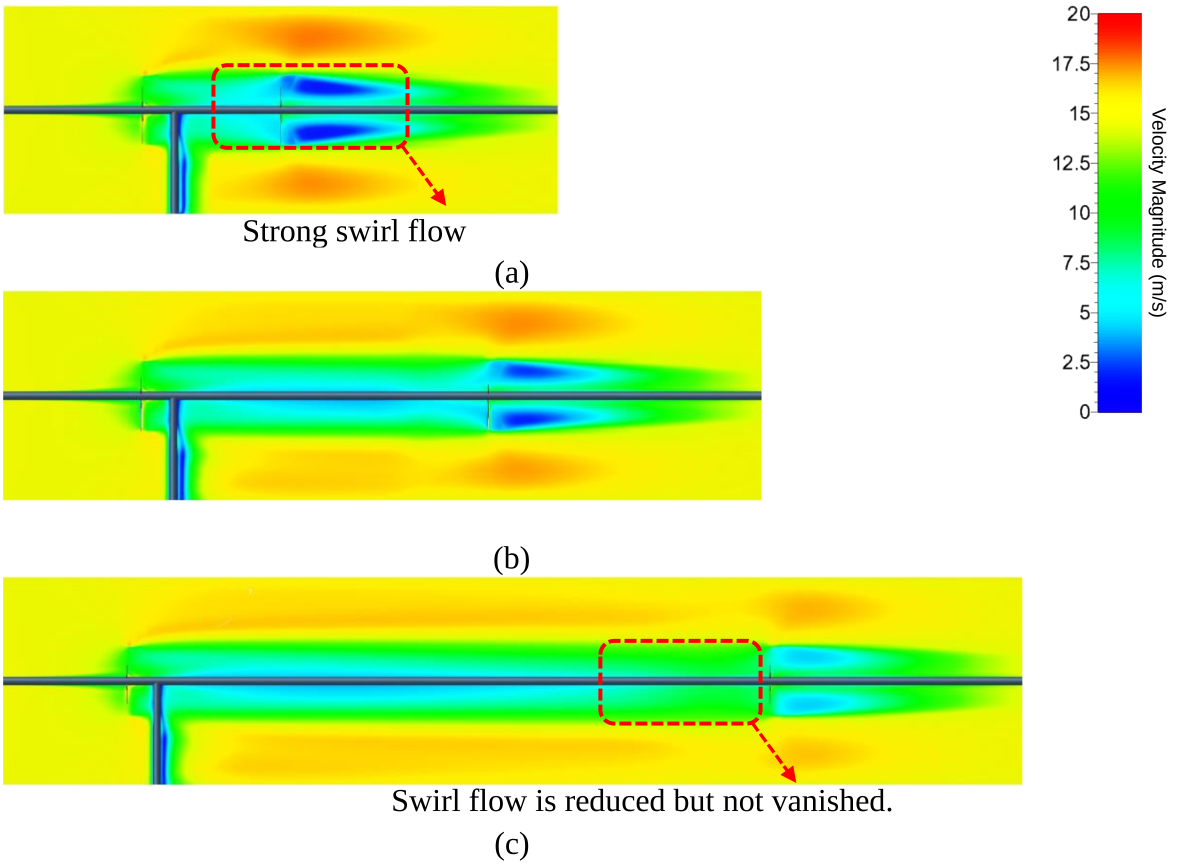

Figure 18. Velocity fields in the meridional view from the case of (a) separation distance = 2D, (b) separation distance = 5D and (c) separation distance = 10D.

Pressure distributions around the aerofoil at the blade mid-span section from both wind turbines are presented in Fig. 19. Generally, the pressure is higher on the pressure side and lower on the suction side of the aerofoil, and the highest-pressure concentration is typically found near the leading edge. In the case of the upstream wind turbine, the highest pressure is observed on the pressure surface near the leading edge. The pressure distributions and the location of the highest-pressure concentration around the aerofoil of the downstream wind turbine depend on the separation distance from the upstream turbine. At the separation distances of 2D and 5D, pressure distribution on both sides of the aerofoil is much lower than that of the upstream turbine, and the highest pressure is seen at the leading edge. In the case of the 10D separation distance, pressure distribution recovers as it is higher than 2D and 5D case but still lower than that of the upstream wind turbine. However, the highest-pressure concentration point shits slightly towards the pressure surface.

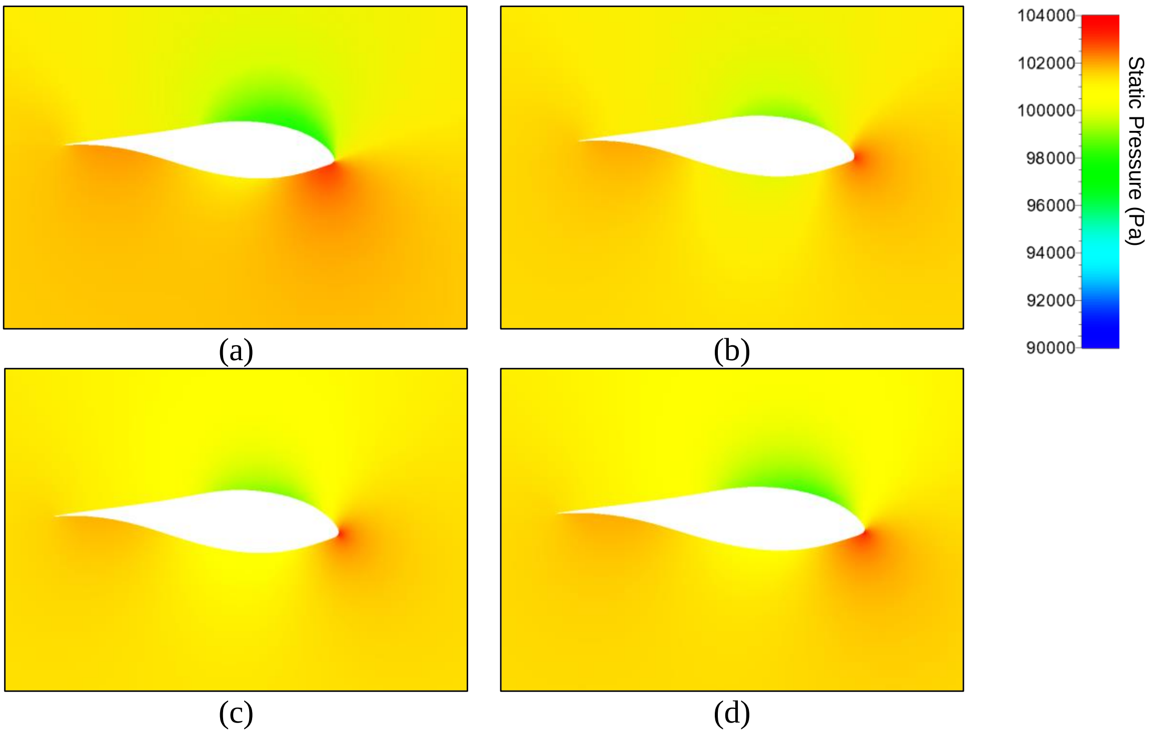

Figure 19. Pressure distributions around the aerofoil at the mid-span section of the blade of (a) the upstream wind turbine, (b) the downstream wind turbine with the separation distance of 2D (c) the downstream wind turbine with the separation distance of 5D and (d) the downstream wind turbine with the separation distance of 10D.

Velocity distributions around the aerofoil at the blade mid-span section from both wind turbines are shown in Fig. 20. In the case of the upstream wind turbine, the high-velocity concentration is seen around the leading edge. After the relative velocity interacts with the blade aerofoil, the velocity is distributed from the pressure surface near the leading edge over to the suction surface up to the half of the chord length. A little flow separation from the suction surface is also seen near the trailing edge. However, in the cases of the downstream wind turbine with separation distances of 2D and 5D, the velocity magnitude is lower than that of the upstream turbine and the velocity distribution is slightly different. The flow interaction point with the blade aerofoil moves towards the leading edge and the velocity is distributed from the leading edge over to the suction surface. The flow separation is very small compared to the upstream turbine. At 10D distance, the velocity magnitude tends to increase again as the wake from the upstream turbine recovers. The flow interaction point shifts a bit towards the pressure surface, and the velocity distribution is similar, but with less magnitude, to that of the upstream turbine.

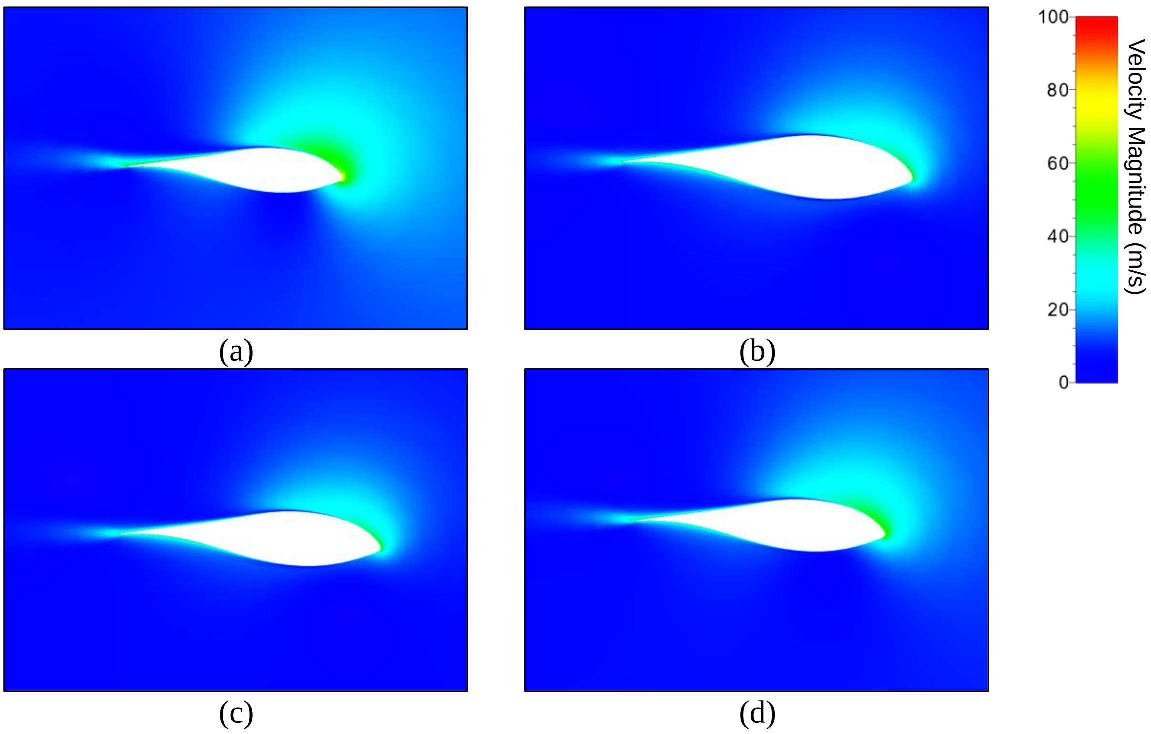

Figure 20. Velocity distributions around the aerofoil at the mid-span section of the blade of (a) the upstream wind turbine, (b) the downstream wind turbine with the separation distance of 2D (c) the downstream wind turbine with the separation distance of 5D and (d) the downstream wind turbine with the separation distance of 10D.

Figure 21 shows the relative velocity streamlines around the aerofoil at the blade mid-span section of both wind turbines. This can be visualised together with the velocity distribution, presented in Fig. 20. The direction of the relative velocity and the flow interaction with the aerofoil are different between the upstream and downstream wind turbines, and they also depend on the separation distances between the turbines. In the case of the upstream wind turbine, the angle of attack is larger than any other cases due to the uniform inflow. The wakes from the upstream wind turbine trigger flow disturbances, which changes the direction of the inflow for the downstream turbines. As a result, the angle of attack for the blade of the downstream wind turbine is smaller than that of the upstream turbine. The angle of attack is much smaller in the cases of 2D and 5D separation distance as the wake from the upstream wind turbine is significant at these distances and the flow around the downstream wind turbine is highly influenced by the wake. However, the angle of attack becomes larger and closer to that of the upstream turbine at 10D distance as the wake from the upstream turbine recovers and the inflow velocity for the downstream turbine is nearly uniform again.

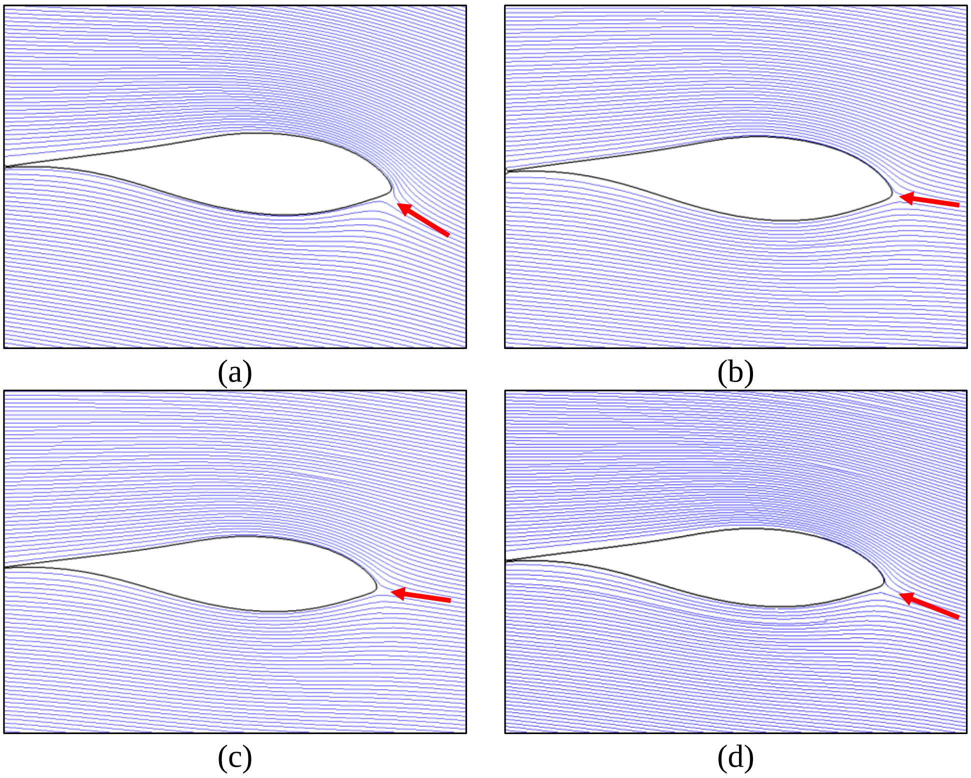

Figure 21. Flow streamlines around the aerofoil at the mid-span section of the blade of (a) the upstream wind turbine, (b) the downstream wind turbine with the separation distance of 2D (c) the downstream wind turbine with the separation distance of 5D and (d) the downstream wind turbine with the separation distance of 10D.

Figure 22 illustrates the relative velocity streamlines in the rotating frame of reference for the upstream and downstream wind turbines. In order to highlight the flow streamlines generated from the upstream wind turbine alone, the streamlines from a single turbine case are presented for the upstream turbine. The streamlines are provided up to 4D downstream of all turbines. The three-dimensional view and meridional view are provided for better visualisation and comparison between different cases. This figure clearly shows the effects of the upstream wind turbine on the flow circulation and wake recovery process behind the downstream wind turbine at different separation distances. Three layers of streamlines from the blade root region, the blade mid-span region and the blade tip region where the tip vortex is generated are presented. In the case of the upstream wind turbine, due to the uniform and steady inflow condition, a recurring pattern of flow streamlines are generated from each layer of the rotor blades. It is also seen that the streamlines are consistent up to 4D distance, which indicates that the downstream wake is still strong. This is also consistent with the aerodynamic parameters of the blades of the downstream turbine placed at 2D and 5D, where the flow is strongly influenced by the wake of the upstream turbine. For the downstream wind turbines, the flow generated from the tip of the blade slightly expands and then gradually becomes smaller as it moves further away from the turbine whereas the flow from the blade root region is circulated around the hub. The major difference between the downstream turbine cases can be seen in the streamlines generated from the blade mid-span region. This is also consistent with the velocity contours presented in Fig. 17 in which it was seen that the velocity fields in the region of 40% - 80% span were significantly affected. In the case of 2D separation distance, the circulation of the flow streamlines from the blade mid-span region suddenly expands by a great extent after leaving the blades which then graduate reduces. Compared to the 2D distance case, the expansion of the flow streamlines is smaller in the 5D distance case whereas no noticeable expansion is observed in the 10D distance case. It is noticed that the streamline behaviours from the 10D distance case tend to be similar, but with some deviations, to those of the upstream turbine because it is placed at a relatively far distance and the inflow condition is more uniform than other two cases. In terms of the wake recover process for the downstream turbine, it is seen that the recovery of the velocity magnitude is shorter in the 5D case than the 2D case. However, in the case of 10D separation distance, the velocity field behind the rotor of the downstream turbine remains relatively greater compared to other two cases due to the nearly uniform inflow, which then gradually recovers to reach the reference velocity in the far downstream region. Therefore, it is now evident that the flow unsteadiness and turbulence resulted from the upstream wind turbine have a great influence on the vortex generation and the wake recovery process of the downstream wind turbine.

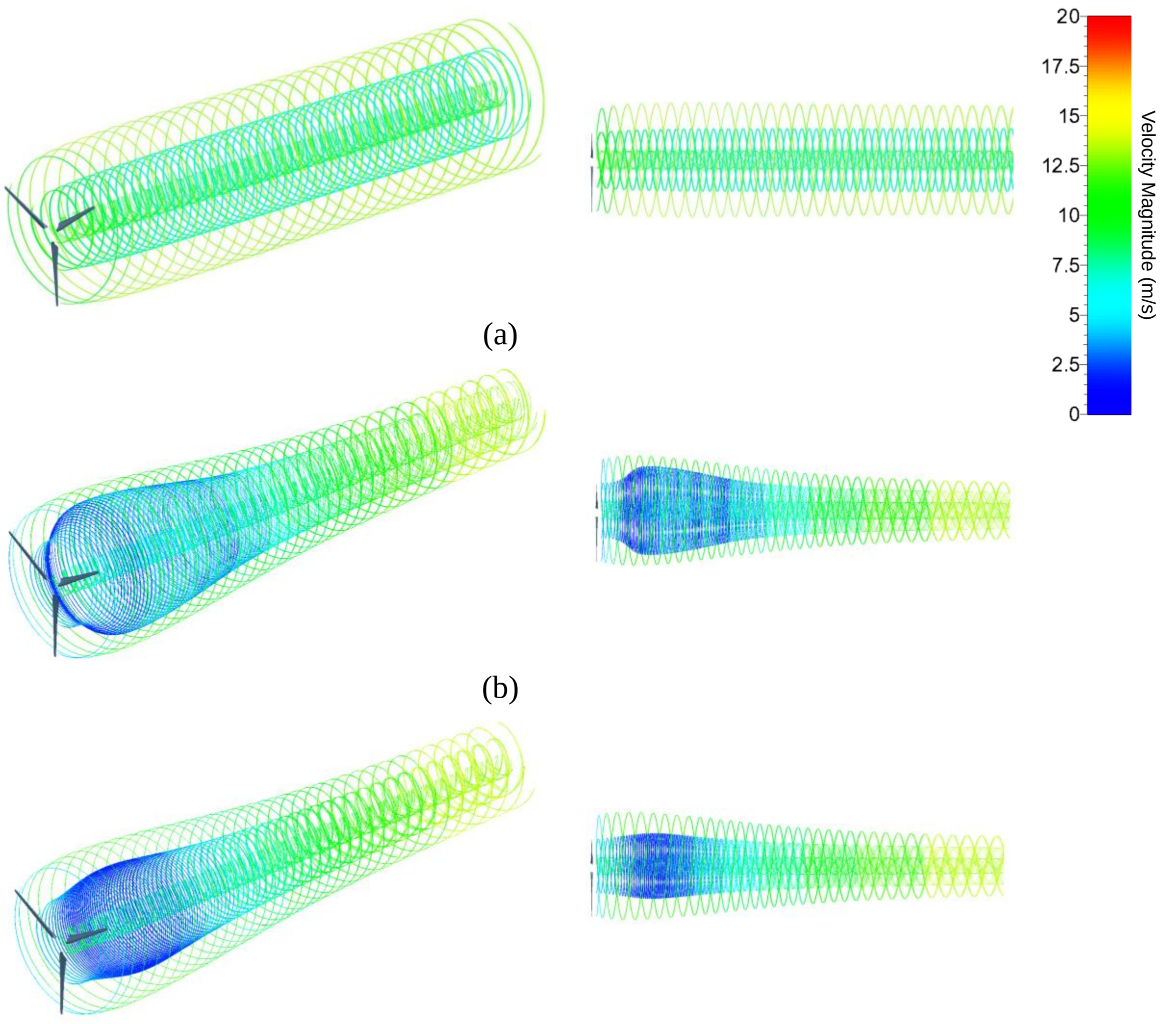

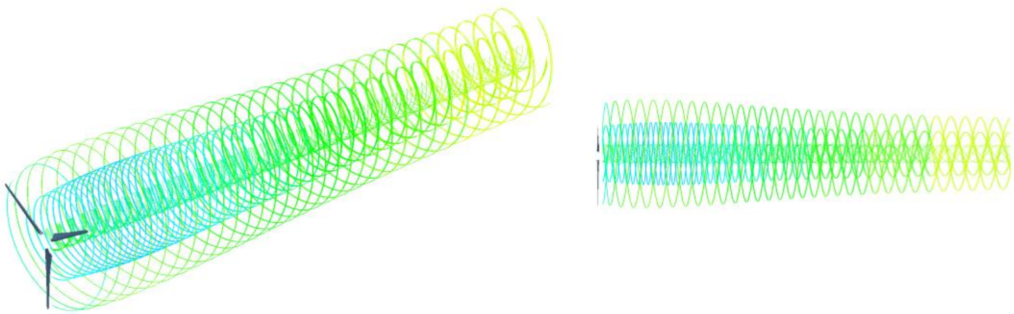

(d)

Figure 22. Flow streamlines generated from (a) the upstream wind turbine, and the downstream wind turbines with the separation distances of (b) 2D, (c) 5D and (d) 10D.

6. CONCLUSIONS

In the present study, numerical simulations have been performed to investigate the effects of separation distances between upstream and downstream wind turbines in arrays on the aerodynamic performances and the flow field around the wind turbines. A novel frequency domain solution method is employed for the first time to model the wind turbines in arrays as a multi-stage turbine in a multi-stage configuration. Before investigating multiple wind turbines, a single wind turbine was first modelled and validated against the experiment and the reference simulation. Good agreements between the numerical results and the experimental data are obtained. The proposed nonlinear frequency domain solution method was then applied to the simulation of two turbines and validated against the conventional time domain solution method based on the 2D separation distance case. The results obtained from both methods are in excellent agreement and they are close to each other.

After the numerical model and method have been validated, the frequency domain method was used for further investigations using different separation distances. It is found that pressure coefficient and skin friction coefficient distributions on the blade surfaces of the downstream wind turbine are significantly influenced by the wake of the upstream wind turbine. The effect of the upstream wake is significant up to the separation distance of 5D and then it gradually reduces. The far wake from the upstream turbine has more effect on the downstream turbine than the near wake. The amplitudes of unsteady fluctuations including pressure and force distribution on the blade surfaces are maximum at the separation distance of 5D. The flow field and wake from the upstream turbine gradually recover beyond the distance of 5D and the aerodynamic performances of the downstream wind turbine tend to increase again. Furthermore, flow visualisations show that the velocity field behind the downstream turbine is most affected in the 40% - 80% span region of the blade rotation and the impact is more significant with smaller separation distances. Therefore, it is certain that the downstream turbine cannot be placed within 5D of the separation distance. Furthermore, according to [6], the minimum spacing restriction of 5D is employed in most recent optimisation studies. Furthermore, it is understood that the common practice for the placement of the downstream wind turbine in most practical applications is around 7D. Hence, a conclusion is drawn based on the results obtained, the reference studies and the common practice that the separation distance should be larger than 5D, and it is recommended that the downstream wind turbine is placed between 5D and 10D to reduce the effect of the upstream turbine as well as to optimise the performances of the downstream turbine and the wind farm.

In terms of the computational cost, the frequency domain solution method can reduce the computation time by one to two orders of magnitude compared to the time domain solution method. Although only the rotor of the downstream turbine is considered in this study, further turbines can be added, and more complex simulations can be performed due to the advantages and capabilities of simulating a series of rotor-stator interactions with the proposed frequency domain solution method.

ACKNOWLEDGEMENTS

The authors would like to acknowledge the financial support received from the Engineering Physics and Science Research Council of the UK (EPSRC EP/R010633/1).

REFERENCES

1. Jain P (2011) Wind Energy Engineering; McGraw-Hill; ISBN: 978-0-07-171478-5.
2. Feng J, Shen W.Z (2017) Design optimization of offshore wind farms with multiple types of wind turbines; Applied Energy; 205: 1283–1297.
3. Chowdhury S, Zhang J, Messac A, Castillo L (2013) Optimizing the arrangement and the selection of turbines for wind farms subject to varying wind conditions; Renewable Energy; 52: 273-282.
4. DuPont B, Cagan J, Moriarty P (2016) An advanced modeling system for optimization of wind farm layout and wind turbine sizing using a multi-level extended pattern search algorithm; Energy; 106: 802-814.
5. Shakoor R, Hassan M.Y, Raheem A, Wu Y.K (2016) Wake effect modelling: A review of wind farm layout optimization using Jensen's model; Renewable and Sustainable Energy Reviews; 58: 1048–1059.
6. Sun H, Yang H, Gao X (2019) Investigation into spacing restriction and layout optimization of wind farm with multiple types of wind turbines; Energy; 168: 637-650.
7. Schepers J.G, Pascal L, Snel H (2010) First results from Mexnext: Analysis of detailed aerodynamic measurements on a 4.5 m diameter rotor placed in the large German Dutch Wind Tunnel DNW; The European Wind Energy Conference and Exhibition (EWEC); April 20-23, Warsaw, Poland.
8. Schepers J.G, Boorsma K, Munduate X (2012) Final Results from Mexnext-I: Analysis of detailed aerodynamic measurements on a 4.5 m diameter rotor placed in the large German

Dutch Wind Tunnel DNW; The Science of making Torque; October 9-11, Oldenburg, Germany.

9. Schepers J.G, Snel H (2007) Model Experiments in Controlled Conditions, Final report; ECN-E-07-042, ECN.
10. Schepers J.G, Boorsma K, Kim C, Cho T (2012) Final report of IEA Task 29, Mexnext (Phase 1): Analysis of Mexico wind tunnel Measurements; ECN-E–12-004, ECN.
11. Krogstad P.Å, Eriksen P.E (2013) "Blind test" calculations of the performance and wake development for a model wind turbine; Renew Energy; 50: 325-33.
12. Pierella F, Krogstad P. Å, Sætran L (2014) Blind Test 2 calculations for two in-line model wind turbines where the downstream turbine operates at various rotational speeds; Renewable Energy; 70: 62-77.
13. O'Brien J.M, Young T.M, O'Mahoney D.C, Griffin P.C (2017) Horizontal axis wind turbine research: A review of commercial CFD, FE codes and experimental practices; Progress in Aerospace Sciences; 92: 1–24.
14. Wang Q, Wang J, Chen J, Luo S, Sun J (2015) Aerodynamic shape optimized design for wind turbine blade using new airfoil series; Journal of Mechanical Science and Technology; 29 (7): 2871-2882.
15. Lee H, Lee D (2019) Numerical investigation of the aerodynamics and wake structures of horizontal axis wind turbines by using nonlinear vortex lattice method; Renewable Energy; 132: 1121-1133.
16. Riziotis V.A, Manolas D.I, Voutsinas S.G (2011) Free-wake Aeroelastic Modelling of Swept Rotor Blades; Conference: EWEA; At Brussels, Belgium.
17. Jeong M.S, Kim S.W, Lee I, Yoo S.J, Park K.C (2013) The impact of yaw error on aeroelastic characteristics of a horizontal axis wind turbine blade; Renewable Energy; 60: 256-268.

18. Rodriguez S.N, Jaworski J.W (2019) Strongly-coupled aeroelastic free-vortex wake framework for floating offshore wind turbine rotors. Part 1: Numerical framework; Renewable Energy; 141: 1127-1145.
19. Rodriguez S.N, Jaworski J.W (2020) Strongly-coupled aeroelastic free-vortex wake framework for floating offshore wind turbine rotors. Part 2: Application; Renewable Energy; 149: 1018-1031.
20. Sørensen J.N, Shen W.Z, Munduate X (1998) Analysis of Wake States by a Full-field Actuator Disc Model; Wind Energy; 1: 73-88.
21. Troldborg N, Sørensen J.N, Mikkelsen R (2007) Actuator Line Simulation of Wake of Wind Turbine Operating in Turbulent Inflow; J. Phys.: Conf. Ser.; 75: 012063.
22. Wang L, Liu X, Kolios A (2016) State of the art in the aero-elasticity of wind turbine blades: Aero-elastic modelling; Renewable and Sustainable Energy Review; 64: 195–210.
23. Kaya M.N, Kose F, Ingham D, Ma L, Pourkashanian M (2018) Aerodynamic performance of a horizontal axis wind turbine with forward and backward swept blades; Journal of Wind Engineering & Industrial Aerodynamics; 176: 166–173.
24. Lee H.M, Kwon O.J (2020) Performance improvement of horizontal axis wind turbines by aerodynamic shape optimization including aeroelastic deformation; Renewable Energy; 147: 2128-2140.
25. Liu Y, Xiao Q, Incecik A, Peyrard C, Wan D (2017) Establishing a fully coupled CFD analysis tool for floating offshore wind turbines; Renewable Energy; 112: 280-301.
26. Wang L, Quant R, Kolios A (2016) Fluid structure interaction modelling of horizontal-axis wind turbine blades based on CFD and FEA; Journal of Wind Engineering & Industrial Aerodynamics; 158: 11-25.

27. Dose B, Rahimi H, Herraez I, Stoevesandt B, Peinke J (2018) Fluid-structure coupled computations of the NREL 5 MW wind turbine by means of CFD; Renewable Energy; 129: 591-605.
28. Yu D.O, Kwon O.J (2014) Predicting wind turbine blade loads and aeroelastic response using a coupled CFD-CSD method; Renewable Energy; 70: 184-196.
29. Dose B, Rahimi H, Stoevesandt B, Peinke J (2020) Fluid-structure coupled investigations of the NREL 5 MW wind turbine for two downwind configurations; Renewable Energy; 146: 1113-1123.
30. Allah V.A, Mayam M.H.S (2017) Large Eddy Simulation of flow around a single and two in-line horizontal-axis wind turbines; Energy; 121: 533-544.
31. Ciri U, Petrolo G, Salvetti M.V, Leonardi S (2017) Large-Eddy Simulations of Two In-Line Turbines in aWind Tunnel with Different Inflow Conditions; Energies; 10 (821): doi:10.3390/en10060821.
32. Choi N.K, Nam S.H, Jeong J.H, Kim K.C (2013) Numerical study on the horizontal axis turbines arrangement in a wind farm: Effect of separation distance on the turbine aerodynamic power output; J. Wind Eng.Ind.Aerodyn.;117: 11–17.
33. Korobenko A, Yan J, Gohari S.M.I, Sarkar S, Bazilevs Y (2017) FSI Simulation of two back-to-back wind turbines in atmospheric boundary layer flow; Computers and Fluids; 158: 167–175.
34. Hall K, Thomas J, Clark W (2002) Computation of Unsteady Nonlinear Flows in Cascades Using a Harmonic Balance Technique; AIAA J.; 40 (5): 879–886.
35. He L (2008) Harmonic Solution of Unsteady Flow Around Blades With Separation; AIAA J.; 46 (6): 1299–1307.

36. Rahmati M.T, He L, Wells R.G (2010) Interface treatment for harmonic solution in multi-row aeromechanic analysis; Proceedings of ASME Turbo Expo 2010: Power for Land, Sea, and Air; June 14-18, Glasgow, UK.
37. Rahmati M.T, He L, Li Y.S (2012) Multi-row interference effects on blade aeromechanics in compressor and turbine stages; 13th International Symposium on Unsteady Aerodynamics, Aeroacoustics and Aeroelasticity of Turbomachines (ISUAAAT); September 11-14, Tokyo, Japan.
38. Nakhchi M.E, Win Naung S, Rahmati M (2020) DNS of secondary flows over oscillating low-pressure turbine using spectral/hp element method; International Journal of Heat and Fluid Flow; 86: 108684.
39. Nakhchi M.E, Win Naung S, Rahmati M (2021) High-resolution direct numerical simulations of flow structure and aerodynamic performance of wind turbine airfoil at wide range of Reynolds numbers; Energy 225: 120261.
40. Win Naung S, Rahmati M, Farokhi H (2021) Direct Numerical Simulation of Interaction between Transient Flow and Blade Structure in a Modern Low-Pressure Turbine; International Journal of Mechanical Sciences; 192: 106104.
41. Win Naung S, Rahmati M.T, Farokhi H (2019) Aerodynamic Analysis of a Wind Turbine with Elevated Inflow Turbulence and Wake using Harmonic Method; Proceedings of the ASME 2019 38th International Conference on Ocean, Offshore and Arctic Engineering (OMAE2019); June 9-14, Glasgow, Scotland.
42. Win Naung S, Rahmati M.T, Farokhi H (2019) Aeromechanical Analysis of Wind Turbines using Non-linear Harmonic Method; Proceedings of the ASME 2019 38th International Conference on Ocean, Offshore and Arctic Engineering (OMAE2019); June 9-14, Glasgow, Scotland.

43. Win Naung S, Rahmati M, Farokhi H (2020) Nonlinear frequency domain solution method for aerodynamic and aeromechanical analysis of wind turbines; Renewable Energy; DOI: https://doi.org/10.1016/j.renene.2020.11.046.
44. Win Naung S, Rahmati M, Farokhi H (2020) Aeromechanical Analysis of a Complete Wind Turbine Using Nonlinear Frequency Domain Solution Method; ASME. J. Eng. Gas Turbines Power; DOI: https://doi.org/10.1115/1.4049206.
45. Rahmati M.T, He L, Li Y.S (2015) The Blade Profile Orientations Effects on the Aeromechanics of Multirow Turbomachines; J. Eng. Gas Turbines Power; 138 (6): 062606.
46. Rahmati M.T, He L, Wang D.X, Li Y.S, Wells R.G, Krishnababu S.K (2014) Nonlinear Time and Frequency Domain Method for Multi-Row Aeromechanical Analysis; ASME J. Turbomach.; 136 (4): 041010.
47. Bechmann A, Sørensen N.N, Zahle F (2011) CFD simulations of the MEXICO rotor; Wind Energy; 14: 677–689.
48. Sørensen N.N, Zahle F, Boorsma K, Schepers G (2016) CFD computations of the second round of MEXICO rotor measurements; Journal of Physics. Conf. Ser.; 753 022054.
49. Herraez I, Medjroubi W, Stoevesandt B, Peinke J (2014) Aerodynamic Simulation of the MEXICO Rotor; Journal of Physics. Conf. Ser.; 555 012051.
50. Plaza B, Bardera R, Visiedo S (2015) Comparison of BEM and CFD results for MEXICO rotor aerodynamics; Journal of Wind Engineering & Industrial Aerodynamics; 145: 115–122.
51. Carrion M, Woodgate M, Steijl R, Barakos G (2014) CFD and Aeroelastic Analysis of the MEXICO Wind Turbine; Journal of Physics. Conf. Ser.; 555 012006.